



# Evaluation of soil carbon simulation in CMIP6 Earth System Models

Rebecca M. Varney<sup>1</sup>, Sarah E. Chadburn<sup>1</sup>, Eleanor J. Burke<sup>2</sup>, and Peter M. Cox<sup>1</sup>

<sup>1</sup>College of Engineering, Mathematics and Physical Sciences, University of Exeter, Laver Building, North Park Road, Exeter, EX4 4QF, UK

<sup>2</sup>Met Office Hadley Centre, FitzRoy Road, Exeter, EX1 3PB, UK

**Correspondence:** Rebecca M. Varney (r.varney@exeter.ac.uk)

**Abstract.** The response of soil carbon represents one of the key uncertainties in future climate change. The ability of Earth System Models (ESMs) to simulate present day soil carbon is therefore vital for reliable projections. In this study the most up-to-date CMIP6 ESMs are evaluated against empirical datasets to assess the ability of each model to simulate soil carbon and related controls: Net Primary Productivity (NPP) and soil carbon turnover time ( $\tau_s$ ). Comparing CMIP6 with CMIP5, uncertainties in modelled soil carbon remain, particularly the underestimation of northern high latitude soil carbon stocks. There is a robust improvement in the simulation of NPP in CMIP6 compared with CMIP5, however the same improvements are not seen in the simulation of  $\tau_s$ . These results suggest a greater emphasis is required on improving the representation of below-ground soil processes in future developments of models. These improvements would help reduce the uncertainty of projected carbon release from global soils under climate change and to increase confidence in the carbon budgets associated with different levels of global warming.

## 1 Introduction

Soil carbon is the Earth's largest terrestrial carbon store, with a magnitude of two to three times the amount of carbon contained within the atmosphere (Jackson et al., 2017). The response of soil carbon to CO<sub>2</sub> induced global warming has the potential to provide a significant feedback on climate change, but this feedback is currently poorly known (Friedlingstein et al., 2006; Gregory et al., 2009; Arora et al., 2013; Friedlingstein et al., 2014; Arora et al., 2020; Song et al., 2021).

Carbon stored within the atmosphere and global soils is exchanged via carbon fluxes, as part of the global carbon cycle (Ciais et al., 2013). The Earth's terrestrial surface has acted as a carbon sink until now (Pan et al., 2011), but there is a possibility of a switch to a source during the 21<sup>st</sup> century, which would accelerate climate change (Cox et al., 2000; Crowther et al., 2016). Due to the significant quantities of carbon stored in soils globally, understanding and quantifying the potential release of carbon from soils is vital if the existing Paris Agreement Targets are to be met (UNFCCC, 2015). Earth System Models (ESMs) are complex numerical models which simulate both climate and carbon cycle processes, and are used to make projections of climate change. The most up-to-date ESMs make up the ensemble known as CMIP6, which is the latest phase of the Coupled Model Inter-comparison Project (CMIP) (Eyring et al., 2016), and is used in the most recent Intergovernmental Panel on Climate Change (IPCC) report (AR6) (IPCC, 2021). The response of the carbon cycle to climate change is fundamental to obtaining



25 accurate future projections, and the relationships between carbon and environmental drivers used in models help to determine this response (Todd-Brown et al., 2013). Therefore, representing present day carbon stores and spatial controls realistically is key for improving the reliability of future projections of climate change.

Present day soil carbon can be approximately broken down into above ground and below ground controls, which influence the spatial distribution of soil carbon stocks (Koven et al., 2015). The above ground control of soil carbon can be considered as the input flux of carbon into the soil from vegetation. Both the amount of carbon from plant and root litter (known as litter fall), and the fraction of this that is converted to longer-lived soil carbon pools, will influence the storage of soil carbon. Net Primary Productivity (NPP) can be used as a proxy for the litter fall flux, where the fluxes are equal when vegetation is in a steady state. The below ground control of soil carbon can be quantified simply in terms of the soil carbon turnover time ( $\tau_s$ ), which is defined as the time carbon resides in the soil (Koven et al., 2017; Carvalhais et al., 2014).  $\tau_s$  can be considered as a proxy for below ground controls on soil carbon storage (Koven et al., 2015).

In this study, the representation of late 20<sup>th</sup> century soil carbon stores and these related controls, NPP and  $\tau_s$ , are evaluated in the latest CMIP6 ESMs. Previously, similar studies have been conducted to evaluate soil carbon in the preceding generations of ESMs, for example: Anav et al. (2013) and Todd-Brown et al. (2013) for CMIP5. There are some existing CMIP6 soil carbon related studies, for example: Arora et al. (2020) evaluate carbon-concentration and carbon-climate feedbacks in 1% CO<sub>2</sub> per year forcing simulations, Burke et al. (2020) evaluates the representation of permafrost in models, and Ito et al. (2020) investigate future soil carbon stocks under specific land-use conditions. This study is the first to specifically focus on global and spatial soil carbon and related controls in CMIP6, with a thorough evaluation against empirical datasets and comparison against the preceding CMIP5 ensemble.

The main results of this study are divided into four sections: (1) Soil carbon stocks, (2) Net Primary Productivity, (3) soil carbon turnover time, and (4) drivers of soil carbon spatial patterns. The first section (1) focuses on soil carbon evaluation on a global and spatial basis, then the second (2) and third (3) sections focus on the evaluation of the related spatial controls of soil carbon, (2) NPP and (3)  $\tau_s$ . The aim of these results sections is to determine where improvements can be seen in CMIP6 compared with CMIP5, and where improvements are still required based on inconsistencies with empirical datasets. The fourth results section (4) moves from the separate evaluation of modelled soil carbon and related controls, to the simulation of the relationships between these variables. The aim of this section is to evaluate the modelled relationships against the equivalent relationships derived from the empirical data - simulating realistic relationships between soil carbon and related drivers will help improve the reliability of future climate change projections. Finally, the discussion provides a breakdown of the main results deduced in this study and identifies key areas for future model development.

## 2 Methods

### 55 2.1 Earth system models

Soil carbon stores and related controls are examined in eleven CMIP6 ESMs (Eyring et al., 2016; Meehl et al., 2014), as shown in Table 1. The ESMs included in this study were chosen due to the availability of the required data in the online repository



at the time of analysis (<https://esgf-node.llnl.gov/search/cmip6/>). In this study, comparisons are made with the previous CMIP generation of ESMs - CMIP5 (Taylor et al., 2012). Similarly, the CMIP5 models included in this study are listed in Table 2.  
60 Again, models were included if the required data was available online (<https://esgf-node.llnl.gov/search/cmip5/>).

Tables 1 (CMIP6) and 2 (CMIP5), present information about the included ESMs, specifically more details about the associated Land Surface Model (LSM). It should be noted that there are similarities between some of the Land Surface Models (LSMs) - either advances from earlier models, or even the same LSM within different ESMs. For example, CESM2 and NorESM2-LM both use the Community Land Model version 5 (CLM5) (Arora et al., 2020). For some modelling centres,  
65 both the CMIP5 and CMIP6 versions of the models are included, and in these cases direct comparisons can be made to determine changes from CMIP5 to CMIP6. These generationally related CMIP5 and CMIP6 models are: CanESM2 and CanESM5, CCSM4 and CESM2, GFDL-ESM2G and GFDL-ESM4, IPSL-CM5A-LR and IPSL-CM6A-LR, MIROC-ESM and MIROC-ES2L, MPI-ESM-LR and MPI-ESM1.2-LR, NorESM1-M and NorESM2-LM, and HadGEM2-ES and UKESM1-0-LL, respectively. The models where only either the CMIP5 or CMIP6 version from the modelling centre was included are: BNU-  
70 ESM and GISS-E2-R from CMIP5 and ACCESS-ESM1.5, BCC-CSM2-MR and CNRM-ESM2-1 from CMIP6. A key general change to note is that CMIP6 has more models that include an interactive nitrogen cycle compared with CMIP5: ACCESS-ESM1.5, CESM2, MIROC-ES2L, MPI-ESM1.2-LR, NorESM2-LM and UKESM1-0-LL in CMIP6 compared with CCSM4 and NorESM1-M in CMIP5. (The CMIP5 model BNU-ESM includes carbon-nitrogen interactions, however this process was turned off in CMIP5 simulations (Ji et al., 2014)). Additionally, an increased number of soil carbon pools is seen in some  
75 CMIP6 models (e.g. CLM5 has 29 carbon pools compared with 20 in CLM4). Arora et al. (2020) include a comprehensive overview of the updates seen in the individual CMIP6 models, which is presented in the ‘Model descriptions’ section of the associated Appendix.

Todd-Brown et al. (2013) include a summary of the temperature and moisture dependencies of soil respiration/decomposition as assumed in the CMIP5 models (see Table 1 of the Todd-Brown et al. (2013) study). The most common representation of the  
80 temperature sensitivity of decomposition is the  $Q_{10}$  equation, which is defined by  $f(T) = Q_{10}^{(T-T_0)/10}$ , where  $T$  is temperature and  $T_0$  is a reference temperature. With the  $Q_{10}$  equation, decomposition increases exponentially with temperature (Davidson and Janssens, 2006). The majority of other models used the Arrhenius equation to represent the temperature sensitivity, where the main difference from the  $Q_{10}$  representation is that decomposition levels off at higher temperature levels (Lloyd and Taylor, 1994). Of the remaining models, the GFDL model simulates an increased decomposition with temperature until some optimal  
85 temperature above which it decreases (Shevliakova et al., 2009) - which Todd-Brown et al. (2013) defined as a ‘hill’ function, and the GISS model implement a linear increase of respiration to temperature up to a maximum value (Del Grosso et al., 2005). The representation of the decomposition sensitivity to soil moisture was found to be to be represented in two ways amongst the CMIP5 models, where either decomposition was assumed to increase monotonically with increasing soil moisture, or less commonly to increase to some optimum moisture level and then decrease (again described as a ‘hill’ function by Todd-Brown  
90 et al. (2013)). In this study we note that the representation of temperature and moisture functions remain similar from CMIP5 from CMIP6. The  $Q_{10}$  equation remains the most common representation of soil temperature sensitivity in models, followed



by the Arrhenius equation and then ‘hill’ functions. Similarly, the most common representation of the sensitivity of soil to moisture in CMIP6 is a monotonically increasing function, followed by ‘hill’ functions of various sorts.

## 2.2 Defining soil carbon variables

95 CMIP defines common output variables (Meehl et al., 2000), which allows for consistent comparison between the models, and for cleaner evaluation of models to observational data. These common output variables also allow for consistent comparison between model generations, in this case between CMIP6 and CMIP5. This study focuses on evaluation of near present day soil carbon and related controls. Therefore the results presented in this study use the CMIP standard historical simulation (CMIP scenario *historical*), for both the CMIP6 and CMIP5 analysis. The historical simulation runs from 1850-2015 in CMIP6 and  
100 from 1850-2005 in CMIP5, where the selected dates for each variable (stated below) were chosen to allow for consistent comparison between CMIP5 and CMIP6, and to best match the modelled data to the observational data.

To evaluate soil carbon, this study uses ‘Soil Carbon’ (CMIP variable *cSoil*) which represents the carbon stored in soils, and where applicable ‘Litter Carbon’ (CMIP variable *cLitter*) which represents carbon stored in the vegetation litter. Total soil carbon,  $C_s$ , is defined to be the sum of these soil carbon and litter carbon variables ( $cSoil + cLitter$ ), where applicable. This  
105 allows for a more consistent comparison between the models and between the models and empirical data, due to differences in how soil carbon and litter carbon are simulated (Todd-Brown et al., 2013; Arora et al., 2020). Where for models that do not report a separate litter carbon pool, the total soil carbon is taken to be simply the *cSoil* variable. Modelled  $C_s$  is time averaged between the years 1950 to 2000 of the historical simulation, and is considered spatially (units of  $\text{kg m}^2$ ), and as global totals (units of  $\text{PgC}$ ), where global totals are calculated as an area weighted sum (using the model land surface fraction,  
110 CMIP variable *sftlf*) and divided by  $1 \times 10^{12}$ ). To calculate northern latitude totals, a sum between the latitudes  $60^\circ \text{ N}$  and  $90^\circ \text{ N}$  is considered.

The CMIP6 models CESM2 and NorESM2-LM have two different variables to represent soil carbon: CMIP variable *cSoil*, which represents the full vertical soil profile, and CMIP variable *cSoilAbove1m*, which represents soil carbon in the top 1m of soil. This is due to the representation of vertically resolved soil carbon in these models, which means there are separate  
115 carbon pools in the model that represent different soil depths (Lawrence et al., 2019). The CMIP variable *cSoilAbove1m* is used throughout this study to represent soil carbon for the models CESM2 and NorESM2-LM, unless otherwise stated. The use of this variable is to enable a more consistent comparison with both the other CMIP6 models and the CMIP5 models. Therefore, an assumption of a 1m depth of soil for modelled soil carbon allows for the fairest evaluation, and evaluation is considered against empirical datasets down to a depth of 1m (see below). However, comparisons with the *cSoil* variable for  
120 both CESM2 and NorESM2-LM are included in Tables 4 and 6 of the Results.

In order to obtain a clean separation between above-ground and below-ground drivers of soil carbon variations, a quasi-equilibrium approximation is made. We begin with the definition of the effective soil carbon turnover time ( $\tau_s$ ) (Varney et al., 2020; Koven et al., 2017; Carvalhais et al., 2014), which represents the average time carbon resides in the soil:

$$\tau_s = C_s / R_h \quad (1)$$



125 where  $R_h$  is the output flux of carbon from the soil, known as the heterotrophic respiration. This definition of the turnover time implicitly neglects other processes that may release soil carbon, but which are not yet routinely included in ESMs (e.g. peat fires or dissolved organic carbon fluxes).

In an unperturbed steady-state (i.e. neglecting disturbances from land-use change, fires, insect outbreaks etc.), there is no net exchange of carbon between land and atmosphere, and  $R_h$  is equal to the Net Primary Productivity (NPP,  $\Pi_N$ ). In the contemporary period, the difference between  $\Pi_N$  and  $R_h$  represents the Net Ecosystem Productivity (NEP,  $\approx 3 \text{ PgC yr}^{-1}$ ), which is small compared to the  $\Pi_N$  and  $R_h$  fluxes ( $\approx 60 \text{ PgC yr}^{-1}$ ). Therefore the present day soil carbon can be approximated by:

$$C_s \approx \Pi_N \tau_s \quad (2)$$

135 which gives a clean separation of soil carbon variation into the above (NPP) and below ( $\tau_s$ ) ground drivers of soil carbon spatial patterns.

To evaluate these soil carbon controls on  $C_{s,eq}$ , NPP and  $\tau_s$  are evaluated separately. This study uses modelled ‘Net Primary Productivity’ (CMIP variable *npp*), which is defined as the mass flux of carbon out of the atmosphere due to NPP on land. NPP is also considered spatially ( $\text{kg m}^{-2} \text{ yr}^{-1}$ ), and as an area weighted global total flux ( $\text{PgC yr}^{-1}$ ). By definition  $\tau_s$  is defined by Eq. 1, so  $\tau_s$  is calculated by soil carbon (as defined above) divided by  $R_h$ .  $R_h$ , ‘Heterotrophic Respiration’ (CMIP variable *rh*), is defined as the mass flux of carbon into the atmosphere due to heterotrophic respiration on land, primarily due to the microbial respiration that occurs in the soil, and where the units of  $R_h$  are the same as that of NPP. The carbon fluxes (NPP and  $R_h$ ) are time averaged over the period 1995-2005 for consistency between the CMIP generations and to match the empirical datasets.  $\tau_s$  can be considered on a spatial level, or as an effective global  $\tau_s$ , which is defined as average  $\tau_s = \text{mean}(C_s) / \text{mean}(R_h)$  (where the mean represents an area weighted global average). The advantage of defining an effective global  $\tau_s$  is that it is not dominated by large spatial outlying values. Using either method, the units for  $\tau_s$  are in years by definition.

145 The relationships of soil carbon,  $C_s$ , NPP and  $\tau_s$ , with both temperature and soil moisture are also considered. For temperature, the variable ‘near surface air temperature’ (CMIP variable *tas*), representing atmospheric temperature at the surface is considered, where the dates 1995-2005 were chosen to be consistent with the carbon fluxes. The variable for atmospheric temperature is considered opposed to soil temperature as equivalent global observational datasets are required for the analysis. For soil moisture, the variable ‘Moisture in Upper Portion of Soil Column’ (CMIP variable *mrsos*), which is defined as the mass content of water in the soil layer in the upper portion of the soil (0cm-10cm depth) is considered, where the dates 1978-2000 were considered to match the empirical data. The standard output *mrsos* is in units of  $\text{kg m}^{-2}$ , however in this study a volumetric soil moisture, referred to as  $\theta$ , is used to allow for consistent comparison with the benchmark data.  $\theta$  is calculated as *mrsos* divided by the depth of the soil layer in mm, which in this case is  $\theta = \text{mrsos} / 100$ . The variable *mrsos* for soil moisture was considered opposed to the full soil column moisture (CMIP variable *mrs0*) as this better matched the available empirical dataset for soil moisture.



## 2.3 Empirical datasets

### 2.3.1 Soil carbon

Observational soil carbon,  $C_s$ , to a depth of 1m, was obtained by combining the empirical Harmonized World Soils Database (HWSD) (FAO and ISRIC, 2012) and Northern Circumpolar Soil Carbon Database (NCSCD) (Hugelius et al., 2013) soil carbon datasets, where NCSCD was used where overlap of the datasets occurs. This is a commonly used method when considering empirical soil carbon and has been previously used in multiple studies, such as: Varney et al. (2020), Koven et al. (2017), and Todd-Brown et al. (2013). This dataset is referred to here as the ‘Benchmark dataset’.

We use the 95% confidence intervals given by Todd-Brown et al. (2013), to derive standard deviations about the global mean soil carbon. To do this, the constructed 95% confidence intervals were used to calculate upper and lower bounds around the mean value. Then assuming the data is normally distributed, these derived 95% confidence intervals were halved to obtain confidence intervals equivalent to a standard deviation error on the mean ( $1412 \pm 215$  PgC). The uncertainty analysis completed in Todd-Brown et al. (2013) is used for the benchmark soil carbon dataset as no quantitative uncertainty has been previously or since defined for the HWSD and NCSCD datasets (Anav et al., 2013).

Additionally, the benchmark dataset was compared with empirical estimates found in the literature to improve the robustness and reliability of the evaluation. Todd-Brown et al. (2013) find that this derived uncertainty is consistent with other empirical estimates of global soil carbon; for example, 1576 PgC in Eswaran et al. (1993), 1220 PgC in Sombroek et al. (1993), and 1502 PgC in Jobbágy and Jackson (2000). This study further compares with empirical estimates of 1395 PgC in Post et al. (1982) and 1515 PgC in Raich and Schlesinger (1992). These empirical estimates are with one standard deviations of the global mean soil carbon given by the benchmark dataset (Table 3).

These additional datasets include: (1) the World Inventory of Soil property Estimates (WISE30sec) dataset down to a depth of 2m (Batjes, 2016), which includes a given standard deviation on the global total soil carbon consistent with our derived benchmark uncertainty, (2) the named ‘S2017’ from Sanderman et al. (2017) soil carbon estimate (1m and 2m), which uses a data-driven statistical model and the History Database of the Global Environment (HYDE) land use data, (3) the Global Soil Dataset for use in Earth System Models (GSDE), which provides a estimates for observational soil carbon down to a depth of up to 2.3m (Shangguan et al., 2014), and (4) the Global Gridded Surfaces of Selected Soil Characteristics (IGBP-DIS) estimate of soil carbon to a depth of 1m, derived by the Oak Ridge National Laboratory Distributed Active Archive Centre (ORNL DAAC) (IGBP, 2000). These datasets were combined to obtain a mean estimate for observational soil carbon down to a depth of 1m, where a global total soil carbon value of  $1560 \pm 214$  PgC was found. This estimate is consistent with our benchmark dataset estimate, and further improves the confidence in our benchmark soil carbon estimate. Furthermore, the spatial correlation coefficients between these additional datasets and our benchmark dataset are considered, where the following values correspond to the above datasets: (1) 0.554, (2) 0.625, (3) 0.482, and (4) 0.622. Map plots comparing the empirical soil carbon datasets are shown in Fig. A1. The estimate for northern latitude total soil carbon has greater uncertainties associated with it, where the standard deviation deduced by combining the empirical datasets is 83 PgC. To account for this increased



190 uncertainty, the deduced standard deviation of 83 PgC is used on the benchmark soil carbon throughout this study, opposed to the 61 PgC derived using the Todd-Brown et al. (2013) uncertainty analysis.

### 2.3.2 Carbon fluxes

To estimate a benchmark Net Primary Production (NPP), the commonly used MODIS NPP (2000–2010) dataset (Zhao et al., 2005) is used. The MODIS NPP dataset does not have associated uncertainty estimates, so this study estimates a standard  
195 deviation error on benchmark NPP as derived by Ito (2011). The MODIS NPP dataset is found to be consistent with 251 empirical present day estimates of NPP found in the literature, which Ito (2011) used to estimate a global value of  $56.2 \pm 14.3$  PgC yr<sup>-1</sup> (compared with a derived MODIS mean value of 56.6 yr<sup>-1</sup>). Moreover, due to the limited choice of observational derived NPP datasets (Harper et al., 2018), models can be further evaluated against using a benchmark dataset for Heterotrophic respiration ( $R_h$ ), where  $R_h$  is estimated using the CARDAMOM (2001–2010) heterotrophic respiration dataset (Bloom et al.,  
200 2015). The empirical CARDAMOM  $R_h$  has associated estimates of error, which were used to derive a standard deviation uncertainty on the empirical average  $R_h$  ( $51.7 \pm 21.8$  PgC yr<sup>-1</sup>). This study includes map plots comparing the two empirical datasets, which is shown in Fig. A2. Global totals for  $R_h$  are also considered for comparison against NPP, where the CMIP6 and CMIP5 values are also shown in Appendix Tables A1 and A2, respectively.

### 2.3.3 Soil carbon turnover time

205 To estimate a benchmark soil carbon turnover time ( $\tau_s$ ), the estimates of observational soil carbon are divided by an estimate of heterotrophic respiration ( $R_h$ ) (see above). To estimate an uncertainty on effective global  $\tau_s$ , this study derived upper ( $\tau_s^+$ ) and lower ( $\tau_s^-$ ) bounds based on the derived  $C_s$  and  $R_h$  uncertainty estimates. The upper bound was calculated using the following:  $\tau_s^+ = C_s^+ / R_h^-$ , where  $C_s^+$  is equal to the mean soil carbon plus one standard deviation and  $R_h^-$  is equal to the mean heterotrophic respiration minus one standard deviation. The lower bound was calculated using the following:  $\tau_s^- =$   
210  $C_s^- / R_h^+$ , where similarly  $C_s^-$  is equal to the mean soil carbon minus one standard deviation and  $R_h^+$  is equal to the mean heterotrophic respiration plus one standard deviation. This method gives a large uncertainty bound around the derived mean estimate ( $27.0_{-11}^{+27}$  yr), so the benchmark data is further compared to empirical estimates. Raich and Schlesinger (1992) derive an estimate of mean soil carbon turnover of 32 yr, using estimates for mean soil carbon pools and mean soil respiration rates. More recently, Carvalhais et al. (2014) derive an estimate for the mean global ecosystem carbon turnover time of  $23_{-4}^{+7}$ , which  
215 is a spatially explicit and observation based estimate. Ito et al. (2020) derived an observational uncertainty range on soil carbon turnover time of 18.5 to 45.8 years, which was derived using similar empirical estimates found in the literature. These estimates give more certainty on the values closer to the derived empirical mean value for  $\tau_s$ .

### 2.3.4 Soil moisture and air temperature

To estimate soil moisture ( $\theta$ ), the Copernicus Climate Change Service (C3S) ‘Soil moisture gridded data from 1978 to present’  
220 dataset (published 2018-10-25) is used, where the years 1978 to 2000 are considered. This dataset is based on the ESA Climate



Change Initiative soil moisture, and estimates global surface soil moisture from a large set of satellite sensors (Copernicus Climate Change Service, 2021; Liu et al., 2011, 2012; Wagner et al., 2012; Gruber et al., 2017; Dorigo et al., 2017). The WFDEI Meteorological Forcing dataset is used to represent observational air temperatures (1995-2005) (Weedon et al., 2014), where dates are chosen to allow for consistency between CMIP generations. This study includes no uncertainty analysis on  
225 the soil moisture and air temperature empirical datasets as these datasets are only used to evaluate spatial correlations with modelled data and not to evaluate soil moisture and air temperature in the models.

## 2.4 Regridding

To allow direct comparisons between the empirical data and model output data, the model data was regridded to match the observational grid. In this case, the observational grid is a  $0.5^\circ$  by  $0.5^\circ$  resolution, 720 longitude and 360 latitude grid. This  
230 was done using Iris - the community-driven Python package for analysing and visualising Earth science data (Met Office, 2010 - 2013). The regridding method assumed conservation of mass and used linear extrapolation, where extrapolation points will be calculated by extending the gradient of the closest two points. Moreover, model land masks are used to calculate the fraction of land in each coastal grid cell.

## 2.5 Statistical analysis

235 It is difficult to evaluate the spatial distributions of modelled soil carbon and related spatial controls against empirical data with a single metric, so the evaluation for both CMIP6 and CMIP5 involves multiple methods. These include: coefficients of variation, spatial standard deviations, spatial Pearson correlation coefficients and Root Mean Square Errors (RMSEs). These methods can be combined to give a more thorough evaluation of spatial soil carbon and associated controls in the CMIP6 models compared to the previous generation of CMIP5 models.

240 The coefficient of variation is defined as the ratio of the ensemble standard deviation (std) to the ensemble mean in each grid cell. This is used to show the amount of variability amongst the models in the ensemble scaled to the size of the ensemble mean, so represents the variability spatially in the ensemble and shows how much variation is present across the ensemble in specific regions. It is presented as hatching on map figures, where shaded 'hatched' regions show regions of high variability within the ensemble. These regions show areas where there is disagreement in the ensemble as there is large spread compared  
245 with the mean, and is defined as where  $std/mean > 0.75$ . The regions where spatial  $C_s < 5 \text{ kg m}^2$  are discounted as the low values of soil carbon discounts the significance of disagreement in these regions.

The spatial standard deviation is a measure of the spread in the data across the globe compared to the mean value. Pearson correlation coefficients (r-values) are used as a spatial measure of the linear correlation between the empirical and modelled data, where a high r-value (near 1 or -1) represents a high correlation in the data and a low r-value (near 0) represents a  
250 negligible correlation. Root Mean Square Error (RMSE) is used as an absolute measure of the difference between the modelled data and empirical data, where the lower the value the lower the difference error. The RMSE can be considered as the standard deviation of the difference, and it is a measure to show the deviation of the modelled data in relation to the empirical data. This statistical data: spatial standard deviations, Pearson correlation coefficients, and RMSEs, can be presented using a Taylor



255 diagram. A Taylor diagram is a mathematical graph used to indicate the performance of a model compared with a benchmark, which in this case is the empirical datasets (Taylor, 2001).

### 3 Results

#### 3.1 Soil carbon stocks: *northern latitude underestimations remain in CMIP6*

##### 3.1.1 Global total evaluation

260 Global total soil carbon (in the top 1m of soil) is shown to vary amongst the ESMs in CMIP6, with a range of 1294 PgC between the models with the lowest and the highest values (Table 4). The global total soil carbon for two (CanESM5 and MIROC-ES2L) out of the eleven CMIP6 models falls within the benchmark soil carbon uncertainty range, 1197 - 1627 PgC (mean  $\pm$  stand deviation). The models with the largest global total soil carbon are CNRM-ESM2-1 (1810 PgC), BCC-CSM2-MR (1770 PgC), and UKESM1-0-LL (1760 PgC), values greater than the benchmark dataset but not the additional empirical datasets (Table 3). The models GFDL-ESM4 (516 PgC) and IPSL-CM6A-LR (639 PgC) have the lowest global total soil carbon values in the ensemble, with global totals significantly lower (approximately 50% less) than the global totals seen in empirical data. It is noted that if the full soil carbon profile is considered for CESM2 and NorESM2-LM opposed to a depth of 1m, the global total soil carbon values are increased to 1870 PgC from 991 PgC in CESM2, and to 2430 PgC from 969 PgC in NorESM2-LM.

270 The ensemble mean global total soil carbon is found to have reduced in CMIP6 from CMIP5. Table 4 includes the CMIP6 ensemble mean global total soil carbon, where a total of  $1206 \pm 445$  PgC is deduced, using regridded model resolutions (see methods). It is noted that Ito (2011) state a CMIP6 ensemble of  $1553 \pm 672$  PgC, however the full soil carbon profile is considered for CESM2 and NorESM2-LM, opposed to a depth of 1m considered in this study. Table 5 shows the CMIP5 equivalent soil carbon values, where an ensemble mean global soil carbon value of  $1480 \pm 810$  PgC is deduced, using equivalent dates in the historical simulation (1950-2000). Todd-Brown et al. (2013) state an ensemble mean soil carbon value of  $1520 \pm 770$  PgC in CMIP5, however the Todd-Brown et al. (2013) study includes the models BCC-CSM1.1, CESM1-CAM5 and INM-CM4, which are missing from the analysis in this study due to data availability. Anav et al. (2013) present a CMIP5 ensemble mean soil carbon value of  $1502 \pm 798$  PgC, but this calculation includes multiple model versions (for example, LR and MR) from the same modelling centre in their ensemble.

280 Despite a reduction in ensemble mean global total soil carbon in CMIP6 compared with CMIP5, the CMIP6 ensemble value remains within the benchmark uncertainty range. However, a significant reduction is seen in the associated standard deviation of the ensemble mean global totals ( $\pm 445$  PgC in CMIP6 from  $\pm 810$  PgC in CMIP5). Moreover, a reduced range of global total values is seen in CMIP6 compared with CMIP5, where a range of 1294 PgC is seen in CMIP6 opposed to 2493 PgC in CMIP5. This suggests that although a significant range in global soil carbon still exists amongst the CMIP6 ESMs, there is an improved consistency between the models seen in CMIP6 compared with the models in CMIP5. It is found from comparing the previous generation models in CMIP5 with the updated CMIP6 equivalent, that multiple models in CMIP6 have lower quantities of soil carbon than in CMIP5, such as: GFDL-ESM4 from GFDL-ESM2G, IPSL-CM6A-LR from IPSL-CM5A-LR,



MIROC-ES2L from MIRCO-ESM and MPI-ESM1.2-LR from MPI-ESM-LR. For example, the CMIP5 model MPI-ESM-LR is reported to have the largest soil carbon magnitude amongst the CMIP5 models, with a global total of 3000 PgC (Table 5), whereas the updated CMIP6 model MPI-ESM1.2-LR has a reduced global total soil carbon value of 970 PgC, amongst the lowest values reported in CMIP6 and below observational derived range (Table 4). Conversely, these reductions are negated in the ensemble mean by the remaining models which have greater quantities of soil carbon in CMIP6 compared to their CMIP5 equivalent, such as CanESM5 from CanESM2, CESM2 from CCSM4, NorESM2-LM from NorESM1-M and UKESM1-0-LL from HadGEM2-ES. For example, the CMIP5 model NorESM1-M is amongst the lowest soil carbon values presented in this ensemble at 538 PgC (Table 5), whereas the updated CMIP6 model NorESM2-LM has an increased global total of 969 PgC (down to 1m) (Table 1).

### 295 3.1.2 Northern latitude total evaluation

Northern latitude soil carbon (down to a depth of 1m, and where northern latitudes defined as 60° N - 90° N) is found to be underestimated in CMIP6, with eight out of the eleven CMIP6 models having lower northern latitude soil carbon values than the derived observational range (Table 4). Two out of eleven CMIP6 models (CNRM-ESM2-1 and MIROC-ES2L) have northern latitude totals that fall within the uncertainty range derived from the benchmark data, 318 - 484 PgC (mean  $\pm$  stand deviation). The CMIP6 models with the greatest northern latitude total soil carbon are BCC-CSM2-MR (575 PgC), CNRM-ESM2-1 (440 PgC), and MIROC-ES2L (347 PgC). The CMIP6 models with the lowest northern latitude soil carbon are IPSL-CM6A-LR (66 PgC), ACCESS-ESM1.5 (151), GFDL-ESM4 (163 PgC), MPI-ESM1.2-LR (175 PgC) and UKESM1-0-LL (194), values significantly lower than the totals seen in empirical data.

The northern latitude soil carbon total was also underestimated in CMIP5, with six out of the ten CMIP5 models estimating northern latitude totals lower than the empirical estimates (Table 5). The ensemble mean total northern latitude soil carbon is lower in CMIP6 ( $266 \pm 139$  PgC seen in Table 4) than in CMIP5 ( $318 \pm 246$  PgC seen in Table 5), which is consistent with the global total results, however both the CMIP5 and CMIP6 mean values fall below the benchmark range. Similarly, as with global soil carbon, a smaller standard deviation on the mean is found for CMIP6 compared with CMIP5. Moreover, there is a reduced range in simulated northern latitude total values amongst the CMIP6 models, where despite a large range seen (66 to 575 PgC), an even greater range is seen in CMIP5 (28.1 to 742 PgC). Moreover, improvements are seen amongst models from CMIP5 to CMIP6. For example, the CMIP5 model NorESM1-M had a northern latitude total soil carbon value of 31.0 PgC, which is significantly lower than what is expected based on the benchmark dataset (Table 5). However, the updated CMIP6 version of this model, NorESM2-LM, has a northern latitude total soil carbon value of 300 PgC, which is much more in line with the expected observational values (Table 4). An improved representation of northern latitude soil carbon is also seen CESM2 (compared with CCSM4), which has the same land surface model as NorESM2-LM (CLM5 (Lawrence et al., 2019)).

The CMIP6 models with the lowest global total values for soil carbon do not always correspond with the lowest northern latitude values for soil carbon. For example, UKESM1-0-LL global total soil carbon is amongst the highest global totals seen in CMIP6, however low quantities of soil carbon are seen in the northern latitudes (approximately 10% of the global total).



320 Conversely, BCC-CSM2-MR, CESM2, GFDL-ESM4, and NorESM2-LM have approximately 30% of their global total stocks in the northern latitude region, which is consistent with the ratio seen in the benchmark dataset. This result suggests that representing global total soil carbon stocks consistent with the benchmark soil carbon, does not imply the consistency in the representation of northern latitude soil carbon stocks, and these should be evaluated separately. However, the large uncertainties associated with the empirical datasets for the northern latitudes are noted (Table 3).

### 325 3.1.3 Spatial evaluation

A lack of consistency in the simulation of soil carbon was found amongst the CMIP5 models, which can be seen in Fig. 1(a), where differences between the empirical and modelled data is shown. Northern latitude soil carbon was found to be underestimated in CMIP5, where areas of blue can be seen in the northern latitudes of the CMIP5 soil carbon map in Fig. 1(a). This underestimation of CMIP5 northern latitude soil carbon is accompanied by significant overestimations seen in mid-  
330 latitude soil carbon. Specifically, large quantities of soil carbon which are inconsistent with our benchmark dataset can be seen in the mid-latitude regions in the following CMIP5 models: CanESM2, GFDL-ESM2G, GISS-E2-R, MIROC-ESM, and MPI-ESM-LR, and less significant overestimations are seen in HadGEM2-ES and IPSL-CM5A-LR (Fig. A3). Systematic errors remain in the CMIP6 models, however there are some improvements seen in the spatial simulation of soil carbon from CMIP5. Soil carbon is still underestimated in the northern latitudes, where the areas of blue still remain the northern  
335 latitudes of the CMIP6 soil carbon map in Fig. 1(a). However, regions of overestimations in the northern latitudes are also seen amongst the CMIP6 models in BCC-CSM2-MR, CESM2, CNRM-ESM2-1, and NorESM2-LM (Fig. 2), but it is noted that this representation might be more consistent with observations if a dataset including deeper soil carbon stocks was considered. CMIP6 shows improvements in the representation of mid-latitude soil carbon, where less of an overestimation is seen in CMIP6 compared with CMIP5 (Fig. 1(a)). This overestimation can still be seen in four of the eleven CMIP6 models: ACCESS-  
340 ESM1.5, CanESM2, MIROC-ES2L and UKESM1-0-LL, however the overestimations in CMIP6 are less inconsistent than when compared with CMIP5 and the number of models showing this limitation in CMIP6 has been reduced (Fig. 2).

Despite the differences seen in the spatial representation of soil carbon between the individual models in CMIP6, the ensemble mean has more areas of agreement within the ensemble compared to the ensemble mean in CMIP5. This can be seen in Fig. 3(a), where there is less hatching (where hatched shaded areas represent regions of low agreement amongst the models in the  
345 ensemble, see methods) in the CMIP6 map compared with the CMIP5 map. Specifically, ensemble mean soil carbon in CMIP6 has more areas of agreement in the mid-latitude region compared with the CMIP5 ensemble mean, where significant areas of disagreement are seen. This disagreement is likely due to the overestimation which exists in some of the CMIP5 models (Fig. A3). Also, a reduction in the area of disagreement is seen in the northern latitudes in CMIP6 compared with CMIP5, however this remains the region where the most disagreement exists across the generations. It is noted that this is a measure of  
350 agreement within the ensemble, and not between the models and empirical data.

The inconsistency of the simulation of spatial soil carbon in CMIP6 is further evaluated using the spatial standard deviations, the spatial Pearson correlation coefficients and Root Mean Square Errors (RMSEs) (see Methods). The Taylor Diagram (Fig. 4(a)) presents all three statistical assessments. The spatial standard deviation for soil carbon is shown on the radial axis between



standard x and y axes in Fig. 4(a). The range of spatial standard deviations amongst the CMIP6 models sees a slight reduction  
355 from the range amongst the CMIP5 models, though significant differences remain. The CMIP6 models CNRM-ESM2-1,  
MIROC-ES2L and UKESM1-0-LL best match the spatial standard deviation derived from the benchmark dataset (Tables 4  
and 5). It is found that the spatial representation of modelled soil carbon in CMIP6 is poorly correlated to the empirical soil  
carbon, where the CMIP6 ensemble spatial correlation coefficient with the empirical data is found to be 0.250. The spatial  
correlation coefficients between the individual CMIP6 and CMIP5 models with the empirical data can also be seen in Fig.  
360 4(a), where the low spatial correlation coefficients are shown by the curved correlation axis. The lowest spatial correlation  
coefficients amongst the CMIP6 models were r-values of 0.104 in IPSL-CM6A-LR and 0.115 in UKESM1-0-LL. The CMIP6  
model that was the most spatially consistent with the empirical data is CNRM-ESM2-1, with an r-value of 0.630. The CMIP6  
ensemble sees a slight reduction in the RMSE compared to the CMIP5 ensemble, suggesting a slight improvement (Fig. 5(a)).  
Significant improvements in the RMSE are seen in MIROC-ES2L from MIROC-ESM and MPI-ESM1.2-LR from MPI-ESM-  
365 LR. These results suggest small improvements in the simulation of soil carbon across this CMIP generation, however the  
low spatial correlation coefficients and variable RMSEs seen across the models in CMIP6 suggest inconsistencies with the  
benchmark data remains.

### 3.2 Net Primary Productivity: *improved in CMIP6 relative to CMIP5*

#### 3.2.1 Global total evaluation

370 Global total NPP amongst the CMIP6 models is consistent with the benchmark dataset (Table 6), where the CMIP6 ensemble  
mean for NPP is approximately 95% of the benchmark mean. The CMIP6 ensemble mean global total NPP ( $53.0 \pm 9.39$  PgC  
 $\text{yr}^{-1}$ ) is found to be slightly lower than the derived mean benchmark value, however it is comfortably within the observational  
uncertainty range ( $56.6 \pm 14.3$  PgC  $\text{yr}^{-1}$ ). The equivalent values for the CMIP5 models can be seen in Table 7, where the  
CMIP5 ensemble total is also found to be within the observational uncertainty range ( $56.3 \pm 15.4$  PgC  $\text{yr}^{-1}$ ). The standard  
375 deviation surrounding the CMIP5 ensemble mean is greater than in CMIP6. This reduced uncertainty in CMIP6 is because  
several of the models have a simulated global total NPP that more closely matches the benchmark NPP global total value  
compared with the previous CMIP5 generation. For example, GFDL-ESM4 from GFDL-ESM2G, IPSL-CM6A-LR from IPSL-  
CM5A-LR, MIROC-ES2L from MIROC-ESM, MPI-ESM1.2-LR from MPI-ESM1-M, and UKESM1-0-LL from HadGEM2-  
ES. The majority of CMIP6 models see a reduction in NPP from the CMIP5 equivalent model, which in general reduces the  
380 overestimation of NPP that was seen in the CMIP5 models (Table 7 and 6). However, it was not the case for CanESM5 from  
CanESM2 which sees an increase in the magnitude of NPP from CMIP5 to CMIP6, resulting in a consequent overestimation  
compared to the benchmark data. A reduced range of modelled global total NPP values is also seen in CMIP6 from CMIP5,  
where the range is reduced from  $48.5$  PgC  $\text{yr}^{-1}$  in CMIP5 to  $32.7$  PgC  $\text{yr}^{-1}$  in CMIP6. These results suggest that overall the  
representation of carbon fluxes in CMIP6 ESMs is more consistent than in CMIP5.



### 385 3.2.2 Spatial evaluation

Modelled NPP in CMIP6 is spatially more consistent with empirical data than CMIP5. This can be seen in Fig. 1(b), where the difference between the modelled and benchmark NPP is shown for both CMIP5 and CMIP6. It can be seen in the CMIP5 map that NPP is overestimated in the tropical regions, specifically in Africa and South East Asia, and the equivalent CMIP6 difference map shows a clear reduction in this overestimation. This tropical overestimation of NPP prominent in CMIP5 (Fig. A4), is still seen in the CMIP6 models CanESM5, MPI-ESM1.2-LR and UKESM1-0-LL. However, this is not seen in the CMIP6 ensemble mean as it is likely negated by underestimations seen in CESM2, CNRM-ESM2-1, and NorESM2-LM (Fig. 6). CMIP6 also sees more consistency with the benchmark dataset in the northern and mid-latitudes compared with CMIP5, where more white areas are seen in the CMIP6 map in Fig. 1(b). An underestimation of NPP is seen in both CMIP5 and CMIP6 on the west side of South America, though unusually high NPP is seen in this region in the MODIS NPP dataset (Fig. A2).  
390 Moreover, greater agreement amongst the models within CMIP6 is seen compared the models in CMIP5. This can be seen in Fig. 3(b), where less hatching representing areas of disagreement within the ensemble is seen in the CMIP6 compared with CMIP5. Specifically, CMIP6 sees less hatching in the northern latitudes, the Middle East and South East Europe, as well as regions in South America, South Africa and Australia.

The improved empirical consistency of modelled NPP in CMIP6 is also found when further evaluated using the same spatial metrics as with soil carbon. Despite a small range remaining in the spatial standard deviations amongst the CMIP6 models (shown by the radial axis in Fig. 4(b)), robust improvements in the spatial correlation coefficients (shown by the curved axis in Fig. 4(b)) and RMSEs are seen across the ensemble compared with CMIP5 (Fig. 5(b)). Notable improvements in the representation of NPP are seen in GFDL-ESM4 compared with GFDL-ESM2G, IPSL-CM6A-LR compared with IPSL-CM5A-LR, and UKESM1-0-LL compared with HadGEM2-ES, with reduced RMSEs seen in each updated model. A general improvement in the spatial correlation coefficients is seen across all the CMIP6 models, where the circle markers (CMIP6 models) in Fig. 4(b), have higher correlation values than the cross markers (CMIP5 models). The general improvement has resulted in the CMIP6 ensemble correlation coefficient (0.836) being greater compared with the equivalent CMIP5 value (0.711). The lowest correlations between modelled and observed NPP amongst the CMIP5 models are GISS-E2-R (0.274) and CanESM2 (0.469). The updated version CanESM5 remains the lowest correlation seen in CMIP6 (0.655), however an improvement in the correlation is seen. The updated version of the GISS model is not included in the CMIP6 ensemble considered in this study, which could be a reason for the increased ensemble mean correlation. However, this effect does not take away from the improvements seen across the CMIP6 models. HadGEM2-ES (0.764) and MPI-ESM-LR (0.764) were the CMIP5 models with the highest correlation to the benchmark NPP, and the updated CMIP6 equivalents of these models remain the models with the greatest correlations, but again improvements in the correlations are seen (0.816 in UKESM1-0-LL and  
415 0.785 MPI-ESM1.2-LR).



### 3.3 Soil carbon turnover time: *no major improvements in CMIP6 compared to CMIP5*

#### 3.3.1 Global evaluation

There are minor improvements seen in the simulated effective global  $\tau_s$  amongst select CMIP6 models (Table 6) compared with CMIP5 (Table 7). The ensemble mean effective global  $\tau_s$  was overestimated in CMIP5 ( $37.8 \pm 19.7$  yr) when compared  
420 with the derived mean  $\tau_s$  using the benchmark datasets ( $27.0^{+27}_{-11}$  yr), which is reduced to a less significant underestimation in CMIP6 ( $23.3 \pm 8.59$  yr). However, both the CMIP5 and CMIP6 estimates fall within the observational uncertainty range. The associated ensemble uncertainty on effective mean  $\tau_s$  is less in CMIP6 compared with CMIP5, with a ensemble standard deviation of approximately 50% less. A significant range is seen in the effective global  $\tau_s$  values amongst the CMIP5 models, with 5 fold difference between the lowest and the highest values (Table 7). This range is mostly due to large overestimations  
425 seen amongst the CMIP5 models, for example in CanESM2, GFDL-ESM2G and MIROC-ESM. A reduced range is seen in amongst the models in CMIP6, however a 4 fold range still exists between the lowest and the highest values (Table 6). This reduced range is partly due to reductions in the effective global  $\tau_s$  values in CMIP6 models compared to the equivalent model in CMIP5, specifically, CanESM5 from CanESM2, GFDL-ESM4 from GFDL-ESM2G, MIROC-ES2L from MIROC-ESM, and MPI-ESM1.2-LR from MPI-ESM-LR. Though overestimations do remain in CMIP6, for example in CNRM-ESM2-1,  
430 where the slowest effective turnover time was seen. Moreover, the range is also reduced due to improvements seen in models which underestimated  $\tau_s$  in CMIP5, such as UKESM1-0-LL from HadGEM2-ES and CESM2 from CCSM4.

#### 3.3.2 Spatial evaluation

The comparison of spatial soil carbon turnover times ( $\tau_s$ ) in CMIP6 with CMIP5 has more varied results than comparing simulated NPP. The CMIP5 ensemble showed an underestimation of  $\tau_s$  in the northern latitudes, which is replaced with an  
435 overestimation of  $\tau_s$  in CMIP6 when compared to the benchmark data (Fig. 1(c)). This northern latitude overestimation in the CMIP6 ensemble is a result of the overestimations of  $\tau_s$  in CESM2 and NorESM2-LM (Fig. 7), which dominate in the CMIP6 ensemble mean. It is noted that this result may differ if deeper soil carbon stocks were considered. The northern latitude underestimation of  $\tau_s$  is still seen within the CMIP6 models, such as CanESM5, CNRM-ESM2-1, GFDL-ESM4, IPSL-CM6A-LR, MIROC-ES2L, MPI-ESM1.2-LR, and UKESM1-0-LL (Fig. 7). An overestimation of mid-latitude  $\tau_s$  was  
440 seen in the CMIP5 models MIROC-ESM and MPI-ESM-LR (Fig. A5), which is no longer seen in the updated CMIP6 models MIROC-ES2L and MPI-ESM1-2-LR, respectively. However, an overestimation of mid-latitude  $\tau_s$  is seen in CMIP6 models BCC-CSM2-MR, CNRM-ESM2-1 and UKESM1-0-LL (Fig. 7). The uncertainty in simulated northern latitude  $\tau_s$  is also apparent in Fig. 3(c), where the hatching shows the lack of agreement within the CMIP6 ensemble in this region. However, more agreement within the CMIP6 ensemble is seen in the same figure in the mid-latitudes and tropical regions compared with  
445 CMIP5.

The simulation of spatial  $\tau_s$  in CMIP6 is further evaluated against the empirical data with the additional statistical metrics. Modelled  $\tau_s$  is found to be poorly spatially correlated to empirical  $\tau_s$  in both the CMIP5 and CMIP6 models (shown by the curved axis in Fig. 4(c)). A slight increase in the ensemble mean spatial correlations is seen from CMIP5 (0.188) to CMIP6



(0.267), due to increases seen amongst individual models between CMIP5 and CMIP6, such as CESM2 from CCSM4, MPI-  
450 ESM1.2-LR from MPI-ESM-LR, and NorESM2-LM from NorESM1-M. However, the consistency of modelled  $\tau_s$  with the  
benchmark datasets remains low. A particularly large range is seen in the spatial standard deviations of  $\tau_s$  amongst the CMIP6  
models, which is an increased range from CMIP5 (shown by the radial axis in Fig. 4(c)). The CMIP6 models with the most  
extreme overestimations of the spatial standard deviations compared to the derived benchmark value (NorESM2-LM, CESM2,  
and ACCESS-ESM1.5), are also found to have large RMSEs (Fig. 5(c)). Amongst the remaining CMIP6 models, the RMSEs  
455 for modelled  $\tau_s$  remain relatively consistent between CMIP5 and CMIP6.

### 3.4 Drivers of soil carbon spatial patterns: *Soil carbon spuriously highly correlated with NPP in CMIP5 and CMIP6*

#### 3.4.1 Global drivers

A negligible correlation ( $\approx 0$ ) is found between the benchmark estimates of soil carbon and NPP, suggesting that soil carbon  
is not spatially correlated to NPP in the real world. On the other hand, soil carbon and NPP ( $C_s$ -NPP) were found to be  
460 significantly correlated in the models in both CMIP5 and CMIP6. The  $C_s$ -NPP spatial correlation was found to be greater  
than 0.5 for six out of the ten CMIP5 ESMs and eight out of the eleven models in CMIP6 (Fig. 8(a)). However, a low spatial  
correlation is found in the CMIP6 models CESM2 (0.134), NorESM2-LM (0.261), and BCC-CSM2-MR (0.214), values most  
consistent with the benchmark datasets. The  $C_s$ - $\tau_s$  spatial correlations found in the CMIP6 models tend to underestimate the  
positive correlation seen in the benchmark datasets (Fig. 8(a)). The majority of CMIP6 models see a negligible or slightly  
465 negative  $C_s$ - $\tau_s$  spatial correlation, despite a low positive correlation produced by the benchmark datasets. The models BCC-  
CSM2-MR, MIROC-ES2L, and NorESM2-LM are most consistent with the benchmark  $C_s$ - $\tau_s$  correlation.

The modelled NPP to temperature (NPP-T) spatial correlations in CMIP6 are consistent with the positive relationship seen  
in the benchmark datasets, however the magnitude of this positive correlation varies amongst the models (Fig. 8(b)). The  
magnitude of the positive NPP-T correlation is underestimated in CanESM5, GFDL-ESM4, and NorESM2-LM, but otherwise  
470 relatively consistent amongst the CMIP6 models. Nonetheless, a much greater range in the modelled NPP-T correlations  
was seen amongst the CMIP5 models, suggesting an improved representation of this relationship in CMIP6. The variation in  
modelled NPP- $\theta$  correlations remains in CMIP6, with models disagreeing in the sign and magnitude of the correlation of NPP  
to soil moisture. The modelled NPP- $\theta$  correlation is the most consistent with the benchmark correlations in GFDL-ESM4,  
MPI-ESM1.2-LR and UKESM1-0-LL (Fig. 8(b)).

475 It is generally agreed across the models in CMIP6 and CMIP5 that  $\tau_s$  and temperature (T) are negatively correlated, with  
the exception of MPI-ESM1.2-LR where a slight positive correlation is seen (Fig. 8(c)). This is consistent with the negative  
 $\tau_s$ -T correlation derived in the benchmark dataset. There is variation amongst the models in the magnitude of the negative  
correlation, with a significant overestimation seen in CanESM5. A negative correlation is also seen in the  $\tau_s$ - $\theta$  correlation  
derived with the benchmark datasets. Inconsistencies with this empirical relationship are seen amongst the models in both  
480 CMIP5 and CMIP6, with many negligible and positive correlations deduced (Fig. 8(c)). The exception is again MPI-ESM1.2-  
LR, which in this case is the model most consistent with the benchmark  $\tau_s$ - $\theta$  correlation.



### 3.4.2 Regional drivers

The spatial correlations of modelled  $C_s$ -NPP are shown to be overestimated at every latitude in both CMIP6 and CMIP5, compared to the equivalent correlations derived from the empirical datasets. It can be seen that the CMIP6 ensemble mean  
485  $C_s$ -NPP correlation has an even larger positive bias compared to the benchmark correlation than in CMIP5. The empirical data sees a reduced  $C_s$ -NPP correlation in the northern latitudes, whereas a slight but less significant reduction is seen in the models (Fig. 9(a)). The spatial correlation between  $C_s$ - $\tau_s$  is shown to vary against latitude in the empirical datasets, where a greater correlation is seen in the tropical and northern latitude regions, and a negligible correlation is seen in the mid-latitudes (Fig. 9(b)). The CMIP6 models simulate the negligible  $C_s$ - $\tau_s$  seen in the mid-latitudes relatively consistently with the benchmark  
490 data, where an improved consistency is seen from CMIP5. However, the CMIP6 models do not simulate the tropical and northern latitude positive  $C_s$ - $\tau_s$  correlations, where a negligible modelled correlation remains in these regions. CMIP5 is more consistent with the benchmark correlations than in CMIP6, where a positive modelled correlation  $C_s$ - $\tau_s$  is seen (Fig. 9(b)).

The spatial correlation between modelled soil carbon and soil moisture ( $C_s$ - $\theta$ ) is consistent with the correlations seen in the benchmark datasets at every latitude, with an improvement seen in the tropical correlation patterns in CMIP6 compared with  
495 CMIP5 (Fig. 9(c)). Both the CMIP5 and CMIP6 ensembles span the benchmark  $C_s$ - $\theta$  correlation, though large model ranges in the  $C_s$ - $\theta$  sensitivity are seen across all latitudes. However, there is a reduced ensemble uncertainty in the  $C_s$ - $\theta$  correlation from CMIP5 to CMIP6 in low and mid latitudes. An overestimation of the negative  $C_s$ -T correlation seen in the benchmark datasets is present in both the CMIP5 and CMIP6 models, except the high latitudes (Fig. 9(d)). This modelled  $C_s$ -T correlation is particularly underestimated in the lower tropical latitudes, where a greater positive correlation is seen here in the benchmark  
500 datasets. Fig. 9(d) suggests a slight improvement in the modelled tropical  $C_s$ -T correlation in CMIP6, and a worsening of modelled  $C_s$ -T in the high latitudes than in CMIP5, when compared to the  $C_s$ -T correlations in the benchmark datasets.

## 4 Discussion

### 4.1 Soil carbon stocks

#### 4.1.1 Global total soil carbon

505 Simulating global soil carbon stocks that are consistent with empirical data is required to predict reliable projections of future soil carbon storage and emission (Todd-Brown et al., 2013). Despite a reduced spread in model estimates of global total soil carbon within CMIP6 relative to CMIP5, discrepancies remain in the consistency of these estimates with the observations between the two CMIP generations. This together with the uncertainty associated with empirical datasets has resulted in no robust conclusion being drawn on the improvement of soil carbon simulation in CMIP6 compared to CMIP5. Due to  
510 the potential significant feedback that exists between soil carbon and global climate, this lack of consistency may reduce our confidence in future projections of climate change (Friedlingstein et al., 2006; Gregory et al., 2009; Arora et al., 2013; Friedlingstein et al., 2014).



#### 4.1.2 Spatial soil carbon patterns

Spatially, the simulation of soil carbon stocks sees some improvement between the CMIP5 and CMIP6 generations. Modelled  
515 soil carbon was found to be poorly spatially correlated with the empirical data amongst models in both CMIP5 and CMIP6 (Fig.  
4(a)). An improvement is seen on the spatial patterns across the mid-latitudes, which were generally overestimated in CMIP5.  
However, significant underestimations of modelled soil carbon in the northern latitudes still remains which has a significant  
impact on model predictions of global total soil carbon stocks (Fig. 1(a)). This systematic underestimation was previously  
reported in the literature as a limitation of the CMIP5 models, where Todd-Brown et al. (2013) found northern latitude soil  
520 carbon to be less consistent with the empirical data than on a global scale. This limitation remains amongst models in the  
CMIP6 generation, where it was found that the majority of CMIP6 models underestimate northern latitude soil carbon stocks  
regardless of whether or not the global soil carbon stocks are underestimated.

An exception to this northern latitude underestimation is seen within CMIP6 in the models CESM2 and NorESM2-LM.  
These ESMs include the Land Surface Model (LSM) CLM5 (Lawrence et al., 2019), which is the first LSM to include the  
525 representation of vertically resolved soil carbon in their CMIP simulations. This representation enables the inclusion of separate  
carbon pools at varying depths in the soil, and allows for an improved simulation of soil carbon stocks (Koven et al., 2013). This  
is of particular importance in the northern latitudes, where carbon stocks are expected to exist at much greater depths than the  
1m considered in this study (Tarnocai et al., 2009; Ran et al., 2021). This can be seen in Table 3, where increased magnitudes  
of soil carbon stocks are shown when increased depths are considered using the empirical datasets. A more thorough evaluation  
530 of soil carbon in both CESM2 and NorESM2-LM is suggested for future research, with a particular focus on this improved  
northern latitude soil carbon stocks simulation, however this evaluation of deeper soil carbon stocks (below 1m) is beyond the  
scope of this study.

Accurately simulating soil carbon in the northern latitude regions is of particular importance as it is a major part of the total  
global soil carbon pool (Jackson et al., 2017). Additionally, much of the carbon stored in these soil is held within permafrost,  
535 which is known to be particularly sensitive to climate change. Permafrost thaw under climate change has the potential to release  
significant amounts of carbon into the atmosphere over a short period of time with increased warming (Schuur et al., 2015;  
Zimov et al., 2006; Burke et al., 2017; Hugelius et al., 2020), representing a significant feedback within the climate system.  
Permafrost dynamics are generally poorly represented in ESMs, where Burke et al. (2020) found CMIP6 ESMs to have a similar  
representation compared to CMIP5. Underestimating soil carbon in the northern latitudes may result in underestimating the  
540 impact of this feedback in future climate change projections. Future improvements are needed to improve the simulation of  
soil carbon stocks globally, but particularly within the northern latitudes.

#### 4.2 Drivers of soil carbon change

To allow for a more in-depth understanding of the inconsistencies found between modelled and empirical soil carbon, the  
simulation of above and below ground controls of soil carbon were also evaluated. Simulations of contemporary soil carbon  
545 can be disaggregated into the effects of litter fall, which is well approximated by plant Net Primary Productivity (NPP), and



effective soil carbon turnover time ( $\tau_s$ ), which is affected by both temperature and moisture of the soil (Koven et al., 2015). If models are to reliably simulate soil carbon in a way that is consistent with empirical data, the spatial drivers of soil carbon, NPP and  $\tau_s$ , must also be simulated consistently with empirical data. Isolating the effects of NPP and  $\tau_s$  on soil carbon helps us to breakdown the simulation of soil carbon to help understand the limitations and inconsistencies seen amongst the models.

#### 550 4.2.1 NPP

A robust improvement in the simulation of NPP is seen in the CMIP6 models compared with the CMIP5 models. This conclusion is deduced by: an increased number of models in CMIP6 have global total NPP values consistent with empirical data (Table 6), the overestimation of tropical NPP amongst CMIP5 models is seen to be reduced amongst the CMIP6 models (Fig. 1(b)), and more agreement is seen within CMIP6 relative to CMIP5 in the simulation of mid and northern latitude NPP (Fig. 3(b)). Modelled NPP was found to be robustly more consistent with the empirical data in CMIP6 compared with CMIP5 in all statistical evaluation metrics. Since CMIP5, multiple models have seen an addition of a dynamic nitrogen cycle (Davies-Barnard et al., 2020), where the models with nitrogen cycles are highlighted in Fig. 5 by the shaded bars. The results suggest an improvement in the simulation of NPP with the addition of dynamic nitrogen in models. However, CMIP6 models that do not represent a nitrogen cycle also mostly see improvements in the simulation of NPP, suggesting NPP is more constrained by observations in the most up to date generation of models. CanESM5 is the only model within CMIP6 to not see an overall improvement in the simulation of NPP, where NPP is found to be overestimated compared with the benchmark dataset. It is likely that the inclusion of a nitrogen cycle in this model would limit this overestimated NPP and improve consistency with the observations (Zhang et al., 2014; Exbrayat et al., 2013).

Despite an improved simulation of NPP in CMIP6, the spatial correlation between modelled soil carbon and NPP was found to be inconsistent with the equivalent empirically derived relationship. This result was previously shown for the CMIP5 models (Todd-Brown et al., 2013), and has been more recently shown for the CMIP6 models (Georgiou et al., 2021), both agreeing with the results found here. The majority of CMIP6 models were found to have positive  $C_s$ -NPP spatial correlations, opposed to a negligible spatial correlation found in the observations (Fig. 8(a)). Despite NPP driving the spatial pattern of soil carbon stocks, a positive correlation is not expected in the real world due to regions with high soil carbon not correlating with regions of high NPP. For example, in the observational derived data soil carbon stocks are greatest in the northern latitudes due to long turnover times in these regions, whereas NPP is lower due to cold temperatures in these regions limiting vegetation growth. The three CMIP6 models which did not significantly overestimate this correlation (CESM2, NorESM2-LM, and BCC-CSM2-MR), are three of the models with the most empirically consistent proportion of soil carbon stocks in the northern latitudes. Conversely the tropical regions see high NPP values, but warmer temperatures result in faster turnover times and lower soil carbon stocks. NPP is expected to increase in the future under climate change (Kimball et al., 1993; Friedlingstein et al., 1995; Amthor, 1995), which means an overly positive correlation in models could result in a subsequent increase in modelled projections of soil carbon stocks. An overestimation of future soil carbon storage could result in an overestimation of the future carbon sink and an inaccurate global carbon budget (Todd-Brown et al., 2013; Friedlingstein et al., 2020).



#### 4.2.2 Soil carbon turnover time

580 The systematic improvements seen in the simulation of NPP in CMIP6 are not seen in the simulation of soil carbon turnover time ( $\tau_s$ ), where the simulation of  $\tau_s$  is found to remain inconsistent with the empirical data in CMIP6. Improvements are seen within CMIP6 relative to CMIP5, such as more agreement within the ensemble in the mid-latitudes and tropical regions, however less agreement is seen in the northern latitudes (Fig. 3(c)). Northern latitude  $\tau_s$  is generally underestimated in models, which corresponds to the underestimation of soil carbon seen in these regions. This has been previously identified in ESMs, where it was found that the underestimation of global  $\tau_s$  amongst the CMIP5 models is primarily due to low values in the northern latitudes (Wu et al., 2018). The reduced agreement in CMIP6 is due to long  $\tau_s$  values existing in the northern latitudes of CESM2 and NorESM2-LM, alongside the general ensemble underestimations (Fig. 7). The increased northern latitude  $\tau_s$  values in CESM2 and NorESM2-LM is likely to be due to the improved representation of soil carbon pools, where vertically resolved soil carbon allows for differential  $\tau_s$  values for pools at varying depths. Despite these individual improvements since 590 CMIP5, large discrepancies exist within the CMIP6 ensemble between modelled and empirical  $\tau_s$ .

To simulate  $\tau_s$  consistently with observations, the relationship of  $\tau_s$  to both temperature (T) and moisture ( $\theta$ ) must also be simulated in a way that is consistent with observations. Generally, the  $\tau_s$ -T relationship is consistently simulated, however there is variation in the modelled temperature sensitivity of  $\tau_s$  across the ensemble. The  $\tau_s$ - $\theta$  relationship is less consistently represented, where the majority of CMIP6 models do not match the empirically derived relationship. Despite a positive dependence 595 of soil respiration on soil moisture, many of the CMIP6 models display a contradictory positive  $\tau_s$ - $\theta$  correlation (Fig. 8). This lack of consistency between the modelled and empirical relationships involving  $\tau_s$ , is likely to be due to key soil processes not being represented. Particularly, a limitation of the  $\tau_s$ - $\theta$  relationship in ESMs is the representation of peat not being simulated. Peat forms in wet areas globally, so to simulate the  $\tau_s$  relationship to soil moisture consistently with empirical data, models must simulate increased, longer turnover times in regions where peat exists. Moreover, to accurately simulate the accumulation 600 of peat in models, the soil column must be vertically resolved to allow for the soil column to grow (Chadburn et al., 2021).

These results suggest much of the uncertainty associated with modelled soil carbon stocks can be attributed to the simulation of below ground processes. The improved consistency of NPP with empirical data suggests considerable efforts have been made to achieve an improved representation of above ground processes in CMIP6 ESMs since the release of the CMIP5 ensemble. However, the same improvements are not seen in the simulation of  $\tau_s$  as systemic limitations remain in the new generation of 605 models, suggesting the same progress on the model development of below ground processes has not been achieved between CMIP5 and CMIP6. Moreover, focus on above ground processes without consideration of below ground processes can result in inconsistencies of soil carbon stocks. For example, the inclusion of a nitrogen cycle has been shown to lead to a reduction in soil carbon in the model, see Fig. 6 in Wiltshire et al. (2021), so tuning of the baseline turnover rates is required to keep soil carbon stocks consistent with observed values.

610 The required improvement of soil carbon pool turnover rates has previously been identified for the CMIP5 ensemble (Nishina et al., 2014), and more recently, Ito et al. (2020) find that the difference in turnover times amongst the CMIP6 models is responsible for approximately 88% of the variation seen in global soil carbon stocks amongst the models, and state that



615 constraining key parameters which control soil carbon turnover processes is a key area for future model development. A key development seen in CMIP6 since CMIP5 is the representation of vertically resolved soil carbon. Models which simulate non-vertically resolved soil carbon typically turn over all the carbon based on the temperature near the soil surface. This could lead to reduced quantities of soil carbon and an underestimation of northern latitude soil carbon stocks, due to near surface soil being warmer than the deeper soil, and as turnover is known to respond exponentially to temperature (Davidson and Janssens, 2006). Overall, further improvements in the representation of soil carbon turnover time, with a particular focus on the northern latitudes, is identified as a key area for future model development.

## 620 5 Conclusions

The ability of Earth System Models (ESMs) to simulate present day soil carbon is vital to help produce reliable projections of climate change. In this study the most up-to-date ESMs, which are part of the CMIP6 ensemble, have been evaluated against empirical datasets to assess their ability to represent soil carbon and related controls: Net Primary Productivity (NPP) and the effective soil carbon turnover time ( $\tau_s = C_s/R_h$ ). The evaluation is completed by comparison to the previous generation of CMIP5 ESMs, to assess where improvements have been made and to identify priorities for future model development. Studies of this type rely on the provided CMIP and empirical data, for which we are thankful. Below the key conclusions from this study are listed:

- 630 1. The spatial patterns of soil carbon in CMIP6 models are more in agreement with each other than they were in CMIP5, and are more consistent with observations in the mid-latitudes. However, soil carbon is still heavily underestimated in high northern latitudes (with the exception of two CMIP6 models that represent deep soil carbon).
2. Overall no significant improvements are seen in the simulation of the observed spatial pattern of soil carbon across the globe from the CMIP5 to the CMIP6 generation.
3. There is good evidence that spatial patterns of contemporary NPP are better simulated in CMIP6 than in CMIP5 generation models, when compared to satellite-derived estimates.
- 635 4. However, spatial patterns of  $\tau_s$  continue to be poorly represented in CMIP6 models, in comparison to estimates derived from observational datasets of soil carbon and heterotrophic respiration ( $R_h$ ).
5. Importantly, soil carbon simulations in both the CMIP5 and CMIP6 ESM generations seem to be spuriously highly-correlated with NPP, which may make soil carbon in these models over responsive to future projected changes in NPP.

Taken together, these conclusions point to a need for a much greater emphasis on improving the representation of below-ground soil processes in next generation (CMIP7) of ESMs.



*Data availability.* The datasets analysed during this study are available online: CMIP5 model output [<https://esgf-node.llnl.gov/search/cmip5/>], CMIP6 model output [<https://esgf-node.llnl.gov/search/cmip6/>], Harmonized World Soils Database (HWSD) and Northern Circumpolar Soil Carbon Database (NCSCD) [[https://github.com/rebeccamayvarney/CMIP\\_soilcarbon\\_evaluation](https://github.com/rebeccamayvarney/CMIP_soilcarbon_evaluation)], World Inventory of Soil property Estimates (WISE30sec) [<https://www.isric.org/explore/wise-databases>], Sanderman et al. 645 2017 soil carbon estimate (1m and 2m) [<https://dataverse.harvard.edu/dataset.xhtml?persistentId=doi:10.7910/DVN/QQQM8V>], Global Soil Dataset for use in Earth System Models (GSDE) [<http://globalchange.bnu.edu.cn/research/soilw/>], Global Gridded Surfaces of Selected Soil Characteristics (IGBP-DIS) [[https://daac.ornl.gov/cgi-bin/dsvviewer.pl?ds\\_id=569](https://daac.ornl.gov/cgi-bin/dsvviewer.pl?ds_id=569)], MODIS Net Primary Production [<https://lpdaac.usgs.gov/products/mod17a3v055/>], CARDAMOM Heterotrophic Respiration [<https://datashare.is.ed.ac.uk/handle/10283/875>], Copernicus Climate Change Service (C3S) soil 650 moisture gridded dataset [[https://cds.climate.copernicus.eu/cdsapp#!/dataset/eu.copernicus.climate.satellite-soil-moisture?tab=overview&utm\\_medium=chatbot&utm\\_source=cds](https://cds.climate.copernicus.eu/cdsapp#!/dataset/eu.copernicus.climate.satellite-soil-moisture?tab=overview&utm_medium=chatbot&utm_source=cds)], and the WFDEI Meteorological Forcing Data [<https://rda.ucar.edu/datasets/ds314.2/>].

*Author contributions.* R.M.V., S.E.C., and P.M.C. outlined the evaluation and drafted the manuscript, and R.M.V. completed the analysis and produced the figures. E.J.B. provided the empirical datasets and gave helpful advice to address the empirical uncertainty. All co-authors 655 provided guidance on the study at various times and suggested edits to the draft manuscript.

*Competing interests.* The authors declare that they have no competing interests.

*Acknowledgements.* This work was supported by the European Research Council ‘Emergent Constraints on Climate-Land feedbacks in the Earth System (ECCLES)’ project, grant agreement number 742472 (R.M.V. and P.M.C.). S.E.C. was supported by a Natural Environment Research Council independent research fellowship, grant no. NE/R015791/1. E.J.B. was supported by the Joint UK BEIS/Defra Met Office 660 Hadley Centre Climate Programme (grant no. GA01101). We acknowledge the World Climate Research Programme’s Working Group on Coupled Modelling, which is responsible for CMIP, and we thank the climate modelling groups for producing and making their model output available to enable studies such as this evaluation study. We also thank providers of empirical datasets, which enabled us to complete the evaluation in this study. The Taylor diagrams presented in this study was produced using code at [<https://gist.github.com/ycopin/3342888>].



## References

- 665 Amthor, J. S.: Terrestrial higher-plant response to increasing atmospheric [CO<sub>2</sub>] in relation to the global carbon cycle, *Global Change Biology*, 1, 243–274, 1995.
- Anav, A., Friedlingstein, P., Kidston, M., Bopp, L., Ciais, P., Cox, P., Jones, C., Jung, M., Myneni, R., and Zhu, Z.: Evaluating the land and ocean components of the global carbon cycle in the CMIP5 Earth System Models, *Journal of Climate*, 26, 6801–6843, 2013.
- Arora, V. and Boer, G.: Uncertainties in the 20th century carbon budget associated with land use change, *Global Change Biology*, 16,  
670 3327–3348, 2010.
- Arora, V., Boer, G., Christian, J., Curry, C., Denman, K., Zahariev, K., Flato, G., Scinocca, J., Merryfield, W., and Lee, W.: The effect of terrestrial photosynthesis down regulation on the twentieth-century carbon budget simulated with the CCCma Earth System Model, *Journal of Climate*, 22, 6066–6088, 2009.
- Arora, V. K., Boer, G. J., Friedlingstein, P., Eby, M., Jones, C. D., Christian, J. R., Bonan, G., Bopp, L., Brovkin, V., Cadule, P., et al.:  
675 Carbon-concentration and carbon-climate feedbacks in CMIP5 Earth system models, *Journal of Climate*, 26, 5289–5314, 2013.
- Arora, V. K., Katavouta, A., Williams, R. G., Jones, C. D., Brovkin, V., Friedlingstein, P., Schwinger, J., Bopp, L., Boucher, O., Cadule, P., et al.: Carbon-concentration and carbon-climate feedbacks in CMIP6 models and their comparison to CMIP5 models, *Biogeosciences*, 17, 4173–4222, 2020.
- Batjes, N. H.: Harmonized soil property values for broad-scale modelling (WISE30sec) with estimates of global soil carbon stocks, *Geoderma*, 269, 61–68, 2016.
- Bentsen, M., Bethke, I., Debernard, J. B., Iversen, T., Kirkevåg, A., Seland, Ø., Drange, H., Roelandt, C., Seierstad, I. A., Hoose, C., et al.: The Norwegian Earth System Model, NorESM1-M–Part 1: description and basic evaluation of the physical climate, *Geoscientific Model Development*, 6, 687–720, 2013.
- Best, M., Pryor, M., Clark, D., Rooney, G., Essery, R., Ménard, C., Edwards, J., Hendry, M., Porson, A., Gedney, N., et al.: The Joint UK  
685 Land Environment Simulator (JULES), model description–Part 1: energy and water fluxes, *Geoscientific Model Development*, 4, 677–699, 2011.
- Bloom, A., Williams, M., et al.: CARDAMOM 2001–2010 global carbon Model-Data Fusion (MDF) analysis, 2015.
- Boucher, O., Servonnat, J., Albright, A. L., Aumont, O., Balkanski, Y., Bastrikov, V., Bekki, S., Bonnet, R., Bony, S., Bopp, L., et al.: Presentation and evaluation of the IPSL-CM6A-LR climate model, *Journal of Advances in Modeling Earth Systems*, 12, e2019MS002010,  
690 2020.
- Burke, E. J., Ekici, A., Huang, Y., Chadburn, S. E., Huntingford, C., Ciais, P., Friedlingstein, P., Peng, S., and Krinner, G.: Quantifying uncertainties of permafrost carbon-climate feedbacks, *Biogeosciences*, 14, 3051–3066, 2017.
- Burke, E. J., Zhang, Y., and Krinner, G.: Evaluating permafrost physics in the Coupled Model Intercomparison Project 6 (CMIP6) models and their sensitivity to climate change, *The Cryosphere*, 14, 3155–3174, 2020.
- 695 Carvalhais, N., Forkel, M., Khomik, M., Bellarby, J., Jung, M., Migliavacca, M., Mu, M., Saatchi, S., Santoro, M., Thurner, M., et al.: Global covariation of carbon turnover times with climate in terrestrial ecosystems, *Nature*, 514, 213, 2014.
- Chadburn, S. E., Burke, E. J., Gallego-Sala, A. V., Smith, N. D., Bret-Harte, M. S., Charman, D. J., Drewer, J., Edgar, C. W., Euskirchen, E. S., Fortuniak, K., et al.: A new approach to simulate peat accumulation, degradation and stability in a global land surface scheme (JULES vn5. 8\_accumulate\_soil), *Geoscientific Model Development Discussions*, pp. 1–34, 2021.



- 700 Cheruy, F., Ducharne, A., Hourdin, F., Musat, I., Vignon, É., Gastineau, G., Bastrikov, V., Vuichard, N., Diallo, B., Dufresne, J.-L., et al.:  
Improved near-surface continental climate in IPSL-CM6A-LR by combined evolutions of atmospheric and land surface physics, *Journal  
of Advances in Modeling Earth Systems*, 12, e2019MS002005, 2020.
- Ciais, P., Sabine, C., Bala, G., Bopp, L., Brovkin, V., Canadell, J., Chhabra, A., DeFries, R., Galloway, J., Heimann, M., Jones, C., Le Quéré,  
C., Myneni, R., Piao, S., and Thornton, P.: Carbon and Other Biogeochemical Cycles, in: *Climate Change 2013: The Physical Science  
705 Basis. Contribution of Working Group I to the Fifth Assessment Report of the Intergovernmental Panel on Climate Change*, edited by  
Stocker, T., Qin, D., Plattner, G.-K., Tignor, M., Allen, S., Boschung, J., Nauels, A., Xia, Y., Bex, V., and Midgley, P., book section 6, pp.  
465–570, Cambridge University Press, Cambridge, United Kingdom and New York, NY, USA, 2013.
- Clark, D., Mercado, L., Sitch, S., Jones, C., Gedney, N., Best, M., Pryor, M., Rooney, G., Essery, R., Blyth, E., et al.: The Joint UK Land  
Environment Simulator (JULES), model description–Part 2: carbon fluxes and vegetation dynamics, *Geoscientific Model Development*,  
710 4, 701–722, 2011.
- Copernicus Climate Change Service, E. K.: Copernicus Climate Change Service, Product User Guide and Specification,  
[https://datastore.copernicus-climate.eu/documents/satellite-soil-moisture/C3S\\_312b\\_Lot4.D3.SM.5-v3.0\\_202101\\_Product\\_User\\_  
Guide\\_Specification\\_i1.0.pdf](https://datastore.copernicus-climate.eu/documents/satellite-soil-moisture/C3S_312b_Lot4.D3.SM.5-v3.0_202101_Product_User_Guide_Specification_i1.0.pdf), 2021.
- Cox, P. M., Betts, R. A., Jones, C. D., Spall, S. A., and Totterdell, I. J.: Acceleration of global warming due to carbon-cycle feedbacks in a  
715 coupled climate model, *Nature*, 408, 184, 2000.
- Crowther, T. W., Todd-Brown, K. E., Rowe, C. W., Wieder, W. R., Carey, J. C., Machmuller, M. B., Snoek, B., Fang, S., Zhou, G., Allison,  
S. D., et al.: Quantifying global soil carbon losses in response to warming, *Nature*, 540, 104, 2016.
- Dai, Y., Zeng, X., Dickinson, R. E., Baker, I., Bonan, G. B., Bosilovich, M. G., Denning, A. S., Dirmeyer, P. A., Houser, P. R., Niu, G., et al.:  
The common land model, *Bulletin of the American Meteorological Society*, 84, 1013–1024, 2003.
- 720 Danabasoglu, G., Lamarque, J.-F., Bacmeister, J., Bailey, D., DuVivier, A., Edwards, J., Emmons, L., Fasullo, J., Garcia, R., Gettelman, A.,  
et al.: The community earth system model version 2 (CESM2), *Journal of Advances in Modeling Earth Systems*, 12, 2020.
- Davidson, E. A. and Janssens, I. A.: Temperature sensitivity of soil carbon decomposition and feedbacks to climate change, *Nature*, 440,  
165, 2006.
- Davies-Barnard, T., Meyerholt, J., Zaehle, S., Friedlingstein, P., Brovkin, V., Fan, Y., Fisher, R. A., Jones, C. D., Lee, H., Peano, D., et al.:  
725 Nitrogen cycling in CMIP6 land surface models: progress and limitations, *Biogeosciences*, 17, 5129–5148, 2020.
- Del Grosso, S., Parton, W., Mosier, A., Holland, E., Pendall, E., Schimel, D., and Ojima, D.: Modeling soil CO<sub>2</sub> emissions from ecosystems,  
*Biogeochemistry*, 73, 71–91, 2005.
- Delire, C., Séférian, R., Decharme, B., Alkama, R., Calvet, J.-C., Carrer, D., Gibelin, A.-L., Joetzjer, E., Morel, X., Rocher, M., et al.:  
The global land carbon cycle simulated with ISBA-CTRIP: Improvements over the last decade, *Journal of Advances in Modeling Earth  
730 Systems*, 12, e2019MS001886, 2020.
- Dorigo, W., Wagner, W., Albergel, C., Albrecht, F., Balsamo, G., Brocca, L., Chung, D., Ertl, M., Forkel, M., Gruber, A., et al.: ESA CCI Soil  
Moisture for improved Earth system understanding: State-of-the art and future directions, *Remote Sensing of Environment*, 203, 185–215,  
2017.
- Dufresne, J.-L., Foujols, M.-A., Denvil, S., Caubel, A., Marti, O., Aumont, O., Balkanski, Y., Bekki, S., Bellenger, H., Benshila, R., et al.:  
735 Climate change projections using the IPSL-CM5 Earth System Model: from CMIP3 to CMIP5, *Climate dynamics*, 40, 2123–2165, 2013.



- Dunne, J., Horowitz, L., Adcroft, A., Ginoux, P., Held, I., John, J., Krasting, J., Malyshev, S., Naik, V., Paulot, F., et al.: The GFDL Earth System Model version 4.1 (GFDL-ESM 4.1): Overall coupled model description and simulation characteristics, *Journal of Advances in Modeling Earth Systems*, 12, e2019MS002015, 2020.
- Dunne, J. P., John, J. G., Adcroft, A. J., Griffies, S. M., Hallberg, R. W., Shevliakova, E., Stouffer, R. J., Cooke, W., Dunne, K. A., Harrison, M. J., et al.: GFDL's ESM2 global coupled climate–carbon earth system models. Part I: Physical formulation and baseline simulation characteristics, *Journal of climate*, 25, 6646–6665, 2012.
- Dunne, J. P., John, J. G., Shevliakova, E., Stouffer, R. J., Krasting, J. P., Malyshev, S. L., Milly, P., Sentman, L. T., Adcroft, A. J., Cooke, W., et al.: GFDL's ESM2 global coupled climate–carbon earth system models. Part II: carbon system formulation and baseline simulation characteristics, *Journal of Climate*, 26, 2247–2267, 2013.
- 745 Eswaran, H., Van Den Berg, E., and Reich, P.: Organic carbon in soils of the world, *Soil science society of America journal*, 57, 192–194, 1993.
- Exbrayat, J.-F., Pitman, A., Zhang, Q., Abramowitz, G., and Wang, Y.-P.: Examining soil carbon uncertainty in a global model: response of microbial decomposition to temperature, moisture and nutrient limitation, *Biogeosciences*, 10, 7095–7108, 2013.
- Eyring, V., Bony, S., Meehl, G. A., Senior, C. A., Stevens, B., Stouffer, R. J., and Taylor, K. E.: Overview of the Coupled Model Intercomparison Project Phase 6 (CMIP6) experimental design and organization, *Geoscientific Model Development (Online)*, 9, 2016.
- 750 FAO, I. and ISRIC, I.: JRC: Harmonized World Soil Database (version 1.2), FAO, Rome, Italy and IIASA, Laxenburg, Austria, 2012.
- Friedlingstein, P., Fung, I., Holland, E., John, J., Brasseur, G., Erickson, D., and Schimel, D.: On the contribution of CO<sub>2</sub> fertilization to the missing biospheric sink, *Global Biogeochemical Cycles*, 9, 541–556, 1995.
- Friedlingstein, P., Cox, P., Betts, R., Bopp, L., von Bloh, W., Brovkin, V., Cadule, P., Doney, S., Eby, M., Fung, I., et al.: Climate–carbon cycle feedback analysis: results from the C4MIP model intercomparison, *Journal of climate*, 19, 3337–3353, 2006.
- 755 Friedlingstein, P., Meinshausen, M., Arora, V. K., Jones, C. D., Anav, A., Liddicoat, S. K., and Knutti, R.: Uncertainties in CMIP5 climate projections due to carbon cycle feedbacks, *Journal of Climate*, 27, 511–526, 2014.
- Friedlingstein, P., O'sullivan, M., Jones, M. W., Andrew, R. M., Hauck, J., Olsen, A., Peters, G. P., Peters, W., Pongratz, J., Sitch, S., et al.: Global carbon budget 2020, *Earth System Science Data*, 12, 3269–3340, 2020.
- 760 Gent, P. R., Danabasoglu, G., Donner, L. J., Holland, M. M., Hunke, E. C., Jayne, S. R., Lawrence, D. M., Neale, R. B., Rasch, P. J., Vertenstein, M., et al.: The community climate system model version 4, *Journal of climate*, 24, 4973–4991, 2011.
- Georgiou, K., Malhotra, A., Wieder, W. R., Ennis, J. H., Hartman, M. D., Sulman, B. N., Berhe, A. A., Grandy, A. S., Kyker-Snowman, E., Lajtha, K., et al.: Divergent controls of soil organic carbon between observations and process-based models, *Biogeochemistry*, 156, 5–17, 2021.
- 765 Goll, D. S., Brovkin, V., Liski, J., Raddatz, T., Thum, T., and Todd-Brown, K. E.: Strong dependence of CO<sub>2</sub> emissions from anthropogenic land cover change on initial land cover and soil carbon parametrization, *Global Biogeochemical Cycles*, 29, 1511–1523, 2015.
- Goll, D. S., Winkler, A. J., Raddatz, T., Dong, N., Prentice, I. C., Ciais, P., and Brovkin, V.: Carbon–nitrogen interactions in idealized simulations with JSBACH (version 3.10), *Geoscientific Model Development*, 10, 2009–2030, 2017.
- Gregory, J. M., Jones, C., Cadule, P., and Friedlingstein, P.: Quantifying carbon cycle feedbacks, *Journal of Climate*, 22, 5232–5250, 2009.
- 770 Gruber, A., Dorigo, W. A., Crow, W., and Wagner, W.: Triple collocation-based merging of satellite soil moisture retrievals, *IEEE Transactions on Geoscience and Remote Sensing*, 55, 6780–6792, 2017.



- Guimberteau, M., Zhu, D., Maignan, F., Huang, Y., Yue, C., Dantec-Nédélec, S., Ottlé, C., Jornet-Puig, A., Bastos, A., Laurent, P., et al.: ORCHIDEE-MICT (v8. 4.1), a land surface model for the high latitudes: model description and validation, *Geoscientific Model Development*, 11, 121–163, 2018.
- 775 Hajima, T., Watanabe, M., Yamamoto, A., Tatebe, H., Noguchi, M. A., Abe, M., Ohgaito, R., Ito, A., Yamazaki, D., Okajima, H., et al.: Development of the MIROC-ES2L Earth system model and the evaluation of biogeochemical processes and feedbacks, *Geoscientific Model Development*, 13, 2197–2244, 2020.
- Harper, A. B., Wiltshire, A. J., Cox, P. M., Friedlingstein, P., Jones, C. D., Mercado, L. M., Sitch, S., Williams, K., and Duran-Rojas, C.: Vegetation distribution and terrestrial carbon cycle in a carbon cycle configuration of JULES4. 6 with new plant functional types, *Geoscientific Model Development*, 11, 2857–2873, 2018.
- 780 Haverd, V., Smith, B., Nieradzik, L., Briggs, P. R., Woodgate, W., Trudinger, C. M., Canadell, J. G., and Cuntz, M.: A new version of the CABLE land surface model (Subversion revision r4601) incorporating land use and land cover change, woody vegetation demography, and a novel optimisation-based approach to plant coordination of photosynthesis, *Geoscientific Model Development*, 11, 2995–3026, 2018.
- Hugelius, G., Tarnocai, C., Broll, G., Canadell, J., Kuhry, P., and Swanson, D.: The Northern Circumpolar Soil Carbon Database: spatially distributed datasets of soil coverage and soil carbon storage in the northern permafrost regions, *Earth System Science Data*, 5, 3–13, 2013.
- 785 Hugelius, G., Loisel, J., Chadburn, S., Jackson, R. B., Jones, M., MacDonald, G., Marushchak, M., Olefeldt, D., Packalen, M., Siewert, M. B., et al.: Large stocks of peatland carbon and nitrogen are vulnerable to permafrost thaw, *Proceedings of the National Academy of Sciences*, 117, 20438–20446, 2020.
- IGBP: Global Gridded Surfaces of Selected Soil Characteristics (IGBP-DIS).[Global Gridded Surfaces of Selected Soil Characteristics (International Geosphere-Biosphere Programme-Data and Information System)], <https://doi.org/10.3334/ORNLDAAAC/569>, 2000.
- IPCC: Full report, in: *Climate Change 2021: The Physical Science Basis. Contribution of Working Group I to the Sixth Assessment Report of the Intergovernmental Panel on Climate Change*, In Press, edited by Masson-Delmotte, V., Zhai, P., Pirani, A., Connors, S., Péan, C., Berger, S., Caud, N., Chen, Y., Goldfarb, L., Gomis, M., Huang, M., Leitzell, K., Lonnoy, E., Matthews, J., Maycock, T., Waterfield, T., Yelekçi, O., Yu, R., and Zhou, B. e., Cambridge University Press, Cambridge, United Kingdom and New York, NY, USA, 2021.
- 795 Ito, A.: A historical meta-analysis of global terrestrial net primary productivity: are estimates converging?, *Global Change Biology*, 17, 3161–3175, 2011.
- Ito, A. and Oikawa, T.: A simulation model of the carbon cycle in land ecosystems (Sim-CYCLE): a description based on dry-matter production theory and plot-scale validation, *Ecological modelling*, 151, 143–176, 2002.
- Ito, A., Hajima, T., Lawrence, D. M., Brovkin, V., Delire, C., Guenet, B., Jones, C. D., Malyshev, S., Matera, S., McDermid, S. P., et al.: Soil carbon sequestration simulated in CMIP6-LUMIP models: implications for climatic mitigation, *Environmental Research Letters*, 15, 124061, 2020.
- 800 Iversen, T., Bentsen, M., Bethke, I., Debernard, J., Kirkevåg, A., Seland, Ø., Drange, H., Kristjansson, J., Medhaug, I., Sand, M., et al.: The Norwegian earth system model, NorESM1-M–Part 2: climate response and scenario projections, *Geoscientific Model Development*, 6, 389–415, 2013.
- 805 Jackson, R. B., Lajtha, K., Crow, S. E., Hugelius, G., Kramer, M. G., and Piñeiro, G.: The ecology of soil carbon: pools, vulnerabilities, and biotic and abiotic controls, *Annual Review of Ecology, Evolution, and Systematics*, 48, 419–445, 2017.
- Ji, D., Wang, L., Feng, J., Wu, Q., Cheng, H., Zhang, Q., Yang, J., Dong, W., Dai, Y., Gong, D., et al.: Description and basic evaluation of Beijing Normal University Earth system model (BNU-ESM) version 1, *Geoscientific Model Development*, 7, 2039–2064, 2014.



- Ji, J., Huang, M., and Li, K.: Prediction of carbon exchanges between China terrestrial ecosystem and atmosphere in 21st century, *Science in China Series D: Earth Sciences*, 51, 885–898, 2008.
- Jobbágy, E. G. and Jackson, R. B.: The vertical distribution of soil organic carbon and its relation to climate and vegetation, *Ecological applications*, 10, 423–436, 2000.
- Jones, C., Hughes, J., Bellouin, N., Hardiman, S., Jones, G., Knight, J., Liddicoat, S., O’connor, F., Andres, R. J., Bell, C., et al.: The HadGEM2-ES implementation of CMIP5 centennial simulations, *Geoscientific Model Development*, 4, 543–570, 2011.
- 815 Kimball, B., Mauney, J., Nakayama, F., and Idso, S.: Effects of increasing atmospheric CO<sub>2</sub> on vegetation, *Vegetatio*, 104, 65–75, 1993.
- Knorr, W.: Annual and interannual CO<sub>2</sub> exchanges of the terrestrial biosphere: Process-based simulations and uncertainties, *Global Ecology and Biogeography*, 9, 225–252, 2000.
- Koven, C., Riley, W., Subin, Z., Tang, J., Torn, M., Collins, W., Bonan, G., Lawrence, D., and Swenson, S.: The effect of vertically resolved soil biogeochemistry and alternate soil C and N models on C dynamics of CLM4, *Biogeosciences*, 10, 7109–7131, 2013.
- 820 Koven, C. D., Chambers, J. Q., Georgiou, K., Knox, R., Negron-Juarez, R., Riley, W. J., Arora, V. K., Brovkin, V., Friedlingstein, P., and Jones, C. D.: Controls on terrestrial carbon feedbacks by productivity versus turnover in the CMIP5 Earth System Models, *Biogeosciences*, 12, 5211–5228, <https://doi.org/10.5194/bg-12-5211-2015>, 2015.
- Koven, C. D., Hugelius, G., Lawrence, D. M., and Wieder, W. R.: Higher climatological temperature sensitivity of soil carbon in cold than warm climates, *Nature Climate Change*, 7, 817, 2017.
- 825 Krinner, G., Viovy, N., de Noblet-Ducoudré, N., Ogée, J., Polcher, J., Friedlingstein, P., Ciais, P., Sitch, S., and Prentice, I. C.: A dynamic global vegetation model for studies of the coupled atmosphere-biosphere system, *Global Biogeochemical Cycles*, 19, 2005.
- Lawrence, D. M., Oleson, K. W., Flanner, M. G., Thornton, P. E., Swenson, S. C., Lawrence, P. J., Zeng, X., Yang, Z.-L., Levis, S., Sakaguchi, K., et al.: Parameterization improvements and functional and structural advances in version 4 of the Community Land Model, *Journal of Advances in Modeling Earth Systems*, 3, 2011.
- 830 Lawrence, D. M., Fisher, R. A., Koven, C. D., Oleson, K. W., Swenson, S. C., Bonan, G., Collier, N., Ghimire, B., Van Kampenhout, L., Kennedy, D., et al.: The Community Land Model version 5: Description of new features, benchmarking, and impact of forcing uncertainty, *Journal of Advances in Modeling Earth Systems*, 11, 4245–4287, 2019.
- Liu, Y., Dorigo, W. A., Parinussa, R., de Jeu, R. A., Wagner, W., McCabe, M. F., Evans, J., and Van Dijk, A.: Trend-preserving blending of passive and active microwave soil moisture retrievals, *Remote Sensing of Environment*, 123, 280–297, 2012.
- 835 Liu, Y. Y., Parinussa, R., Dorigo, W. A., De Jeu, R. A., Wagner, W., Van Dijk, A., McCabe, M. F., and Evans, J.: Developing an improved soil moisture dataset by blending passive and active microwave satellite-based retrievals, *Hydrology and Earth System Sciences*, 15, 425–436, 2011.
- Lloyd, J. and Taylor, J.: On the temperature dependence of soil respiration, *Functional ecology*, pp. 315–323, 1994.
- Mauritsen, T., Bader, J., Becker, T., Behrens, J., Bittner, M., Brokopf, R., Brovkin, V., Claussen, M., Crueger, T., Esch, M., et al.: Developments in the MPI-M Earth System Model version 1.2 (MPI-ESM1.2) and its response to increasing CO<sub>2</sub>, *Journal of Advances in Modeling Earth Systems*, 11, 998–1038, 2019.
- 840 Meehl, G. A., Boer, G. J., Covey, C., Latif, M., and Stouffer, R. J.: The coupled model intercomparison project (CMIP), *Bulletin of the American Meteorological Society*, 81, 313–318, 2000.
- Meehl, G. A., Moss, R., Taylor, K. E., Eyring, V., Stouffer, R. J., Bony, S., and Stevens, B.: Climate model intercomparisons: Preparing for  
845 the next phase, *Eos, Transactions American Geophysical Union*, 95, 77–78, 2014.



- Melton, J. R., Arora, V. K., Wisernig-Cojoc, E., Seiler, C., Fortier, M., Chan, E., and Teckentrup, L.: CLASSIC v1. 0: the open-source community successor to the Canadian Land Surface Scheme (CLASS) and the Canadian Terrestrial Ecosystem Model (CTEM)–Part 1: Model framework and site-level performance, *Geoscientific Model Development*, 13, 2825–2850, 2020.
- Met Office: Iris: A Python package for analysing and visualising meteorological and oceanographic data sets, Exeter, Devon, v1.2 edn.,  
850 <http://scitools.org.uk/>, 2010 - 2013.
- Nishina, K., Ito, A., Beerling, D., Cadule, P., Ciais, P., Clark, D., Falloon, P., Friend, A., Kahana, R., Kato, E., et al.: Quantifying uncertainties in soil carbon responses to changes in global mean temperature and precipitation, *Earth System Dynamics*, 5, 197–209, 2014.
- Pan, Y., Birdsey, R. A., Fang, J., Houghton, R., Kauppi, P. E., Kurz, W. A., Phillips, O. L., Shvidenko, A., Lewis, S. L., Canadell, J. G., et al.: A large and persistent carbon sink in the world's forests, *Science*, 333, 988–993, 2011.
- 855 Post, W. M., Emanuel, W. R., Zinke, P. J., and Stangenberger, A. G.: Soil carbon pools and world life zones, *Nature*, 298, 156–159, 1982.
- Raddatz, T., Reick, C., Knorr, W., Kattge, J., Roeckner, E., Schnur, R., Schnitzler, K.-G., Wetzell, P., and Jungclaus, J.: Will the tropical land biosphere dominate the climate–carbon cycle feedback during the twenty-first century?, *Climate dynamics*, 29, 565–574, 2007.
- Raich, J. W. and Schlesinger, W. H.: The global carbon dioxide flux in soil respiration and its relationship to vegetation and climate, *Tellus B*, 44, 81–99, 1992.
- 860 Ran, Y., Li, X., Cheng, G., Che, J., Aalto, J., Karjalainen, O., Hjort, J., Luoto, M., Jin, H., Obu, J., et al.: New high-resolution estimates of the permafrost thermal state and hydrothermal conditions over the Northern Hemisphere, *Earth System Science Data Discussions*, pp. 1–27, 2021.
- Sanderman, J., Hengl, T., and Fiske, G. J.: Soil carbon debt of 12,000 years of human land use, *Proceedings of the National Academy of Sciences*, 114, 9575–9580, 2017.
- 865 Sato, H., Itoh, A., and Kohyama, T.: SEIB–DGVM: A new Dynamic Global Vegetation Model using a spatially explicit individual-based approach, *Ecological Modelling*, 200, 279–307, 2007.
- Schmidt, G. A., Kelley, M., Nazarenko, L., Ruedy, R., Russell, G. L., Aleinov, I., Bauer, M., Bauer, S. E., Bhat, M. K., Bleck, R., et al.: Configuration and assessment of the GISS ModelE2 contributions to the CMIP5 archive, *Journal of Advances in Modeling Earth Systems*, 6, 141–184, 2014.
- 870 Schuur, E. A., McGuire, A. D., Schädel, C., Grosse, G., Harden, J. W., Hayes, D. J., Hugelius, G., Koven, C. D., Kuhry, P., Lawrence, D. M., et al.: Climate change and the permafrost carbon feedback, *Nature*, 520, 171–179, 2015.
- Séférian, R., Nabat, P., Michou, M., Saint-Martin, D., Voldoire, A., Colin, J., Decharme, B., Delire, C., Berthet, S., Chevallier, M., et al.: Evaluation of CNRM earth system model, CNRM-ESM2-1: Role of earth system processes in present-day and future climate, *Journal of Advances in Modeling Earth Systems*, 11, 4182–4227, 2019.
- 875 Seiler, C., Melton, J. R., Arora, V. K., and Wang, L.: CLASSIC v1. 0: the open-source community successor to the Canadian Land Surface Scheme (CLASS) and the Canadian Terrestrial Ecosystem Model (CTEM)–Part 2: Global benchmarking, *Geoscientific Model Development*, 14, 2371–2417, 2021.
- Seland, Ø., Bentsen, M., Olivié, D., Toniazzo, T., Gjermundsen, A., Graff, L. S., Debernard, J. B., Gupta, A. K., He, Y.-C., Kirkevåg, A., et al.: Overview of the Norwegian Earth System Model (NorESM2) and key climate response of CMIP6 DECK, historical, and scenario  
880 simulations, *Geoscientific Model Development*, 13, 6165–6200, 2020.
- Sellar, A. A., Walton, J., Jones, C. G., Wood, R., Abraham, N. L., Andrejczuk, M., Andrews, M. B., Andrews, T., Archibald, A. T., de Mora, L., et al.: Implementation of UK Earth system models for CMIP6, *Journal of Advances in Modeling Earth Systems*, 12, e2019MS001 946, 2020.



- 885 Shanguan, W., Dai, Y., Duan, Q., Liu, B., and Yuan, H.: A global soil data set for earth system modeling, *Journal of Advances in Modeling Earth Systems*, 6, 249–263, 2014.
- Shevliakova, E., Pacala, S. W., Malyshev, S., Hurtt, G. C., Milly, P., Caspersen, J. P., Sentman, L. T., Fisk, J. P., Wirth, C., and Crevoisier, C.: Carbon cycling under 300 years of land use change: Importance of the secondary vegetation sink, *Global Biogeochemical Cycles*, 23, 2009.
- 890 Sombroek, W. G., Nachtergaele, F. O., and Hebel, A.: Amounts, dynamics and sequestering of carbon in tropical and subtropical soils, *Ambio (Journal of the Human Environment, Research and Management)*; (Sweden), 22, 1993.
- Song, X., Wang, D.-Y., Li, F., and Zeng, X.-D.: Evaluating the performance of CMIP6 Earth system models in simulating global vegetation structure and distribution, *Advances in Climate Change Research*, 12, 584–595, 2021.
- Swart, N. C., Cole, J. N., Kharin, V. V., Lazare, M., Scinocca, J. F., Gillett, N. P., Anstey, J., Arora, V., Christian, J. R., Hanna, S., et al.: The Canadian earth system model version 5 (CanESM5. 0.3), *Geoscientific Model Development*, 12, 4823–4873, 2019.
- 895 Tarnocai, C., Canadell, J., Schuur, E. A., Kuhry, P., Mazhitova, G., and Zimov, S.: Soil organic carbon pools in the northern circumpolar permafrost region, *Global biogeochemical cycles*, 23, 2009.
- Taylor, K. E.: Summarizing multiple aspects of model performance in a single diagram, *Journal of Geophysical Research: Atmospheres*, 106, 7183–7192, 2001.
- 900 Taylor, K. E., Stouffer, R. J., and Meehl, G. A.: An overview of CMIP5 and the experiment design, *Bulletin of the American Meteorological Society*, 93, 485–498, 2012.
- Todd-Brown, K., Randerson, J., Post, W., Hoffman, F., Tarnocai, C., Schuur, E., and Allison, S.: Causes of variation in soil carbon simulations from CMIP5 Earth system models and comparison with observations, *Biogeosciences*, 10, 1717–1736, 2013.
- Trudinger, C. M., Haverd, V., Briggs, P. R., and Canadell, J. G.: Interannual variability in Australia’s terrestrial carbon cycle constrained by multiple observation types, *Biogeosciences*, 13, 6363–6383, 2016.
- 905 UNFCCC: Adoption of The Paris Agreement FCCC/CP/2015/L.9/Rev.1, <http://unfccc.int/resource/docs/2015/cop21/eng/109r01.pdf>, 2015.
- Varney, R. M., Chadburn, S. E., Friedlingstein, P., Burke, E. J., Koven, C. D., Hugelius, G., and Cox, P. M.: A spatial emergent constraint on the sensitivity of soil carbon turnover to global warming, *Nature communications*, 11, 1–8, 2020.
- Wagner, W., Dorigo, W., de Jeu, R., Fernandez, D., Benveniste, J., Haas, E., Ertl, M., et al.: Fusion of active and passive microwave observations to create an essential climate variable data record on soil moisture, *ISPRS Annals of the Photogrammetry, Remote Sensing and Spatial Information Sciences (ISPRS Annals)*, 7, 315–321, 2012.
- 910 Watanabe, S., Hajima, T., Sudo, K., Nagashima, T., Takemura, T., Okajima, H., Nozawa, T., Kawase, H., Abe, M., Yokohata, T., et al.: MIROC-ESM 2010: Model description and basic results of CMIP5-20c3m experiments, *Geoscientific Model Development*, 4, 845–872, 2011.
- Weedon, G. P., Balsamo, G., Bellouin, N., Gomes, S., Best, M. J., and Viterbo, P.: The WFDEI meteorological forcing data set: WATCH Forcing Data methodology applied to ERA-Interim reanalysis data, *Water Resources Research*, 50, 7505–7514, 2014.
- 915 Wiltshire, A. J., Burke, E. J., Chadburn, S. E., Jones, C. D., Cox, P. M., Davies-Barnard, T., Friedlingstein, P., Harper, A. B., Liddicoat, S., Sitch, S., et al.: JULES-CN: a coupled terrestrial carbon–nitrogen scheme (JULES vn5. 1), *Geoscientific Model Development*, 14, 2161–2186, 2021.
- 920 Wu, D., Piao, S., Liu, Y., Ciais, P., and Yao, Y.: Evaluation of CMIP5 earth system models for the spatial patterns of biomass and soil carbon turnover times and their linkage with climate, *Journal of Climate*, 31, 5947–5960, 2018.



- Wu, T., Lu, Y., Fang, Y., Xin, X., Li, L., Li, W., Jie, W., Zhang, J., Liu, Y., Zhang, L., et al.: The Beijing Climate Center climate system model (BCC-CSM): The main progress from CMIP5 to CMIP6, *Geoscientific Model Development*, 12, 1573–1600, 2019.
- Yue, X. and Unger, N.: The Yale Interactive terrestrial Biosphere model version 1.0: description, evaluation and implementation into NASA GISS ModelE2, *Geoscientific Model Development*, 8, 2399–2417, 2015.
- 925 Zhang, Q., Wang, Y.-P., Matear, R., Pitman, A., and Dai, Y.: Nitrogen and phosphorous limitations significantly reduce future allowable CO<sub>2</sub> emissions, *Geophysical Research Letters*, 41, 632–637, 2014.
- Zhao, M., Heinsch, F. A., Nemani, R. R., and Running, S. W.: Improvements of the MODIS terrestrial gross and net primary production global data set, *Remote sensing of Environment*, 95, 164–176, 2005.
- 930 Zhao, M., Golaz, J.-C., Held, I., Guo, H., Balaji, V., Benson, R., Chen, J.-H., Chen, X., Donner, L., Dunne, J., et al.: The GFDL global atmosphere and land model AM4. 0/LM4. 0: 2. Model description, sensitivity studies, and tuning strategies, *Journal of Advances in Modeling Earth Systems*, 10, 735–769, 2018.
- Ziehn, T., Chamberlain, M. A., Law, R. M., Lenton, A., Bodman, R. W., Dix, M., Stevens, L., Wang, Y.-P., and Sribnovsky, J.: The Australian Earth System Model: ACCESS-ESM1. 5, *Journal of Southern Hemisphere Earth Systems Science*, 70, 193–214, 2020.
- Zimov, S. A., Schuur, E. A., and Chapin III, F. S.: Permafrost and the global carbon budget, *Science(Washington)*, 312, 1612–1613, 2006.

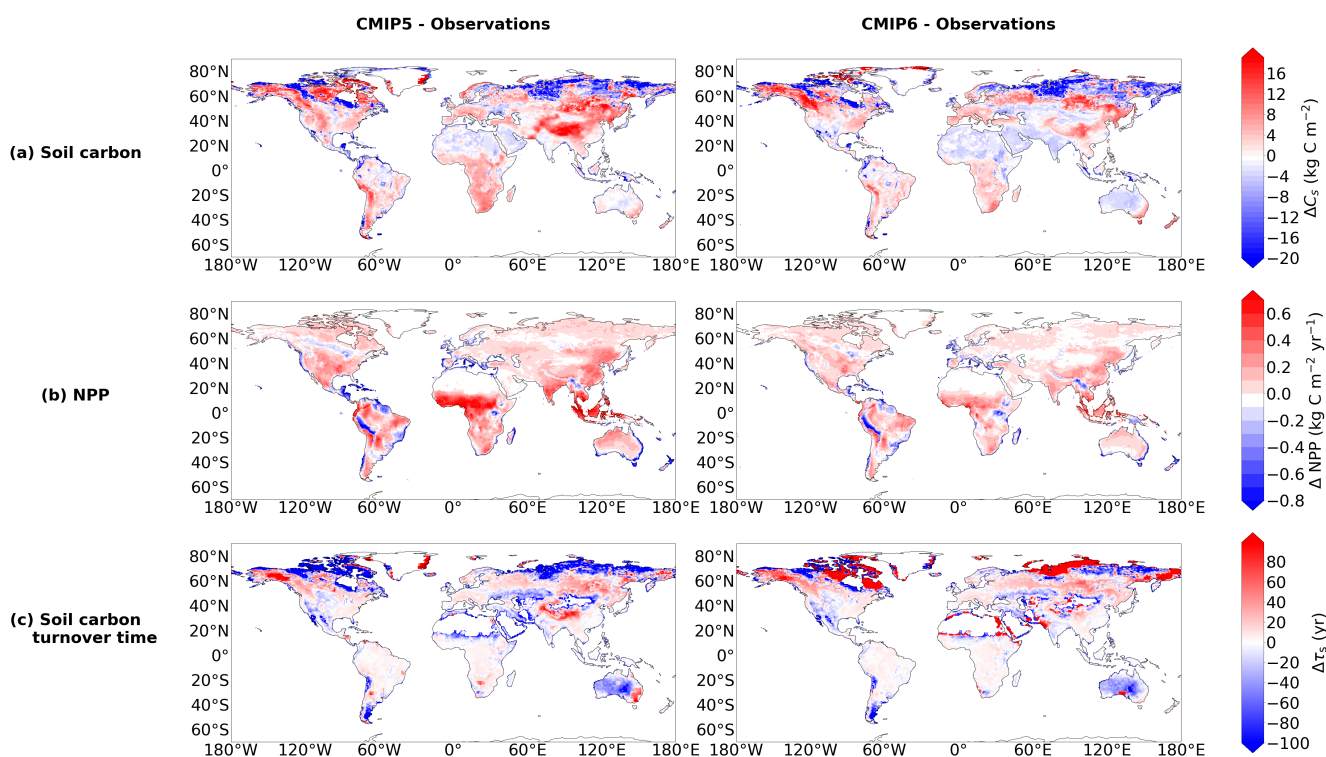


**Figure 1.** Maps presenting the difference between the modelled and benchmark data for the CMIP5 and CMIP6 ensembles, for: (a)  $C_s$  ( $\text{kg m}^{-2}$ ), (b) NPP ( $\text{kg m}^{-2} \text{ yr}^{-1}$ ), and (c)  $\tau_s$  (yr).

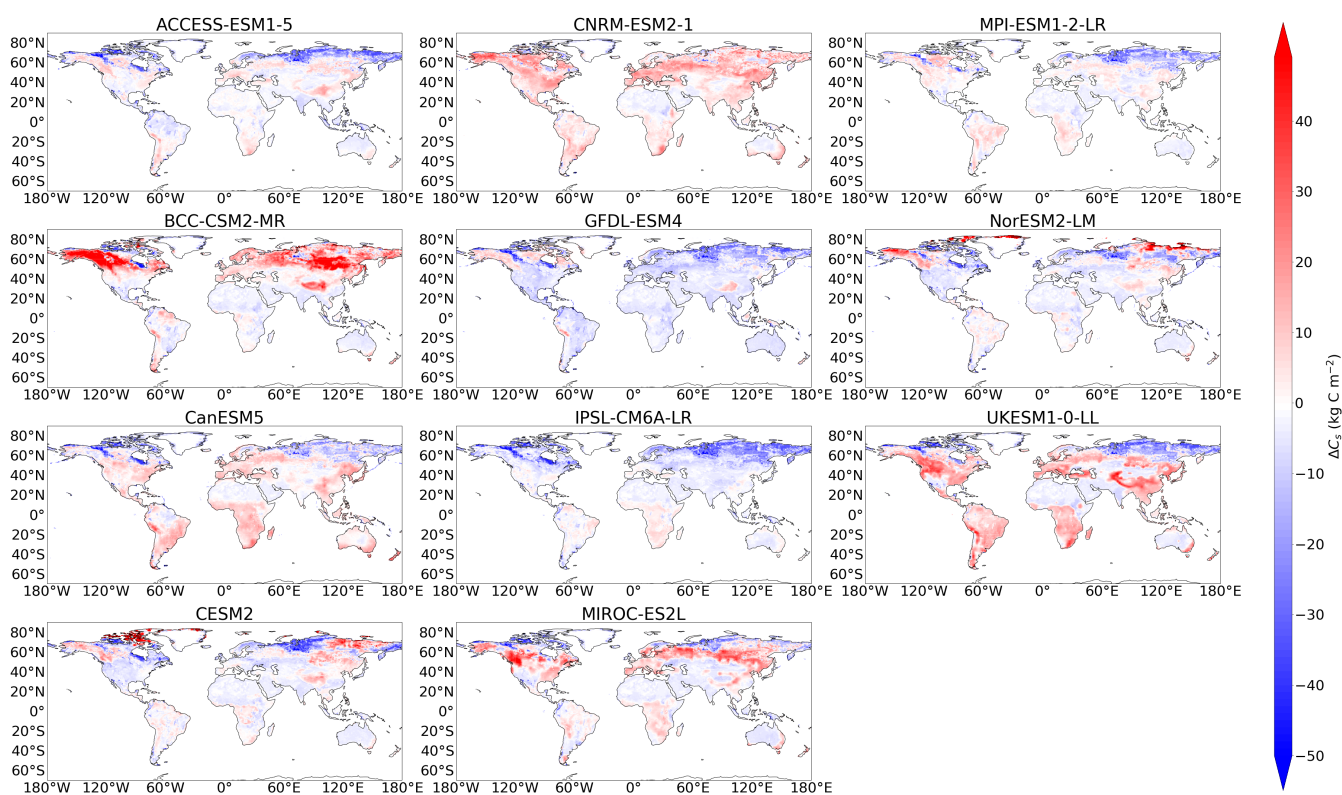


**Figure 2.** Maps of the difference in soil carbon ( $C_s$ ) between the historical simulation of each CMIP6 model and the benchmark data.

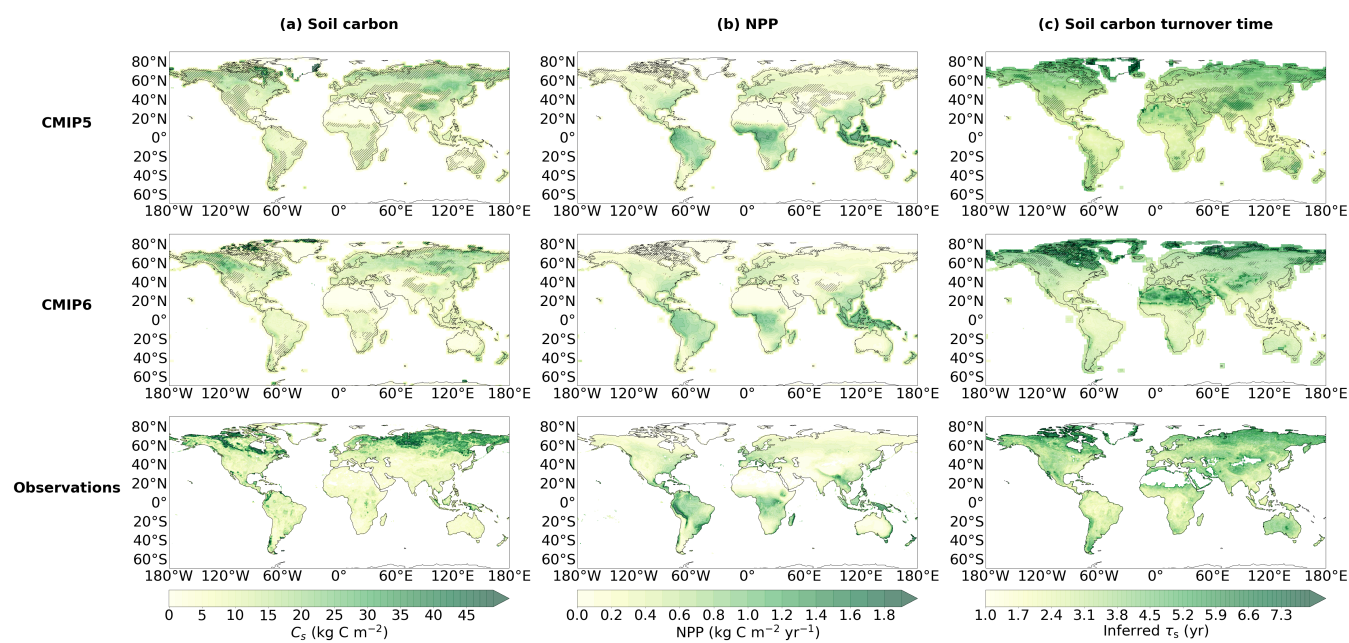


**Figure 3.** Ensemble mean maps for (a)  $C_s$  ( $\text{kg m}^{-2}$ ), (b) NPP ( $\text{kg m}^{-2} \text{ yr}^{-1}$ ), and (c)  $\tau_s$  (yr), presented for the CMIP6 ensemble, CMIP5 ensemble and the benchmark datasets. The hatched areas are used to show regions of low agreement within the ensemble, where regions of low soil carbon ( $< 5 \text{ kg m}^{-2}$ ) have been excluded.

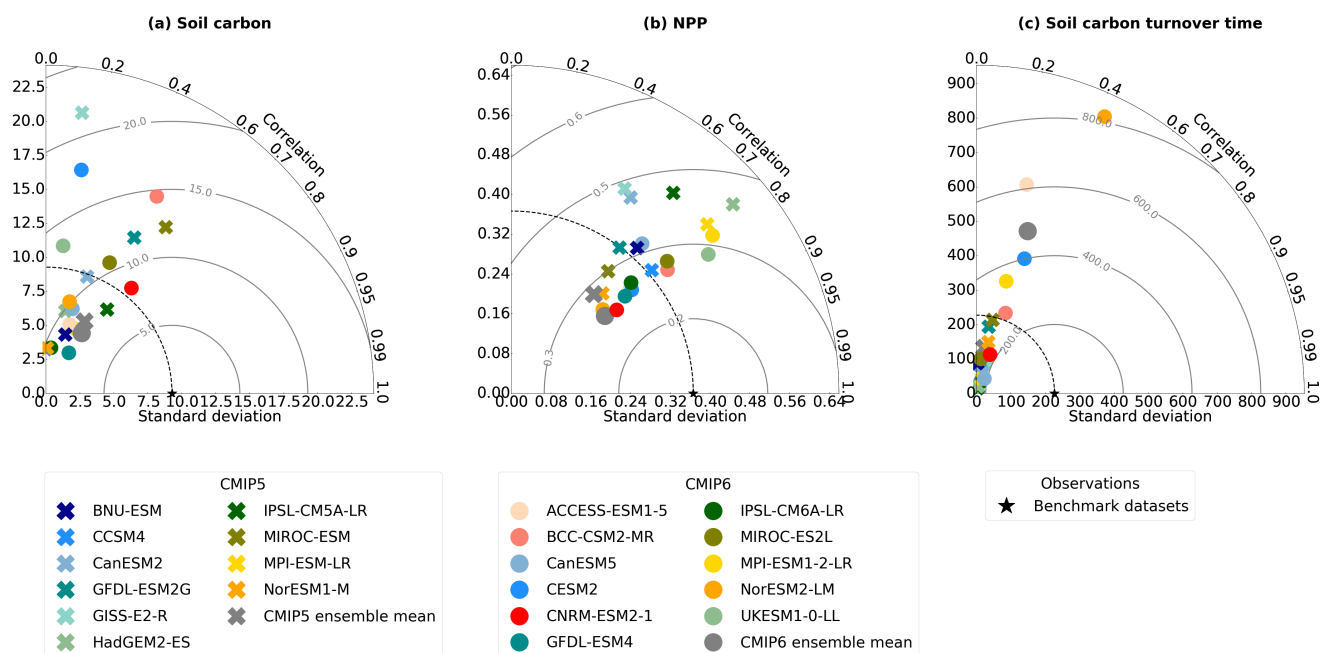


**Figure 4.** Taylor diagrams showing the spatial standard deviation (shown by the radial axis between standard x and y axes), the Pearson correlation coefficients (shown by the curved correlation axis), and the RMSE (shown by the grey contours), for the ESMs in both CMIP5 and CMIP6 compared to the benchmark datasets, for (a) soil carbon ( $C_s$ ), (b) NPP, and (c) soil carbon turnover time ( $\tau_s$ ).

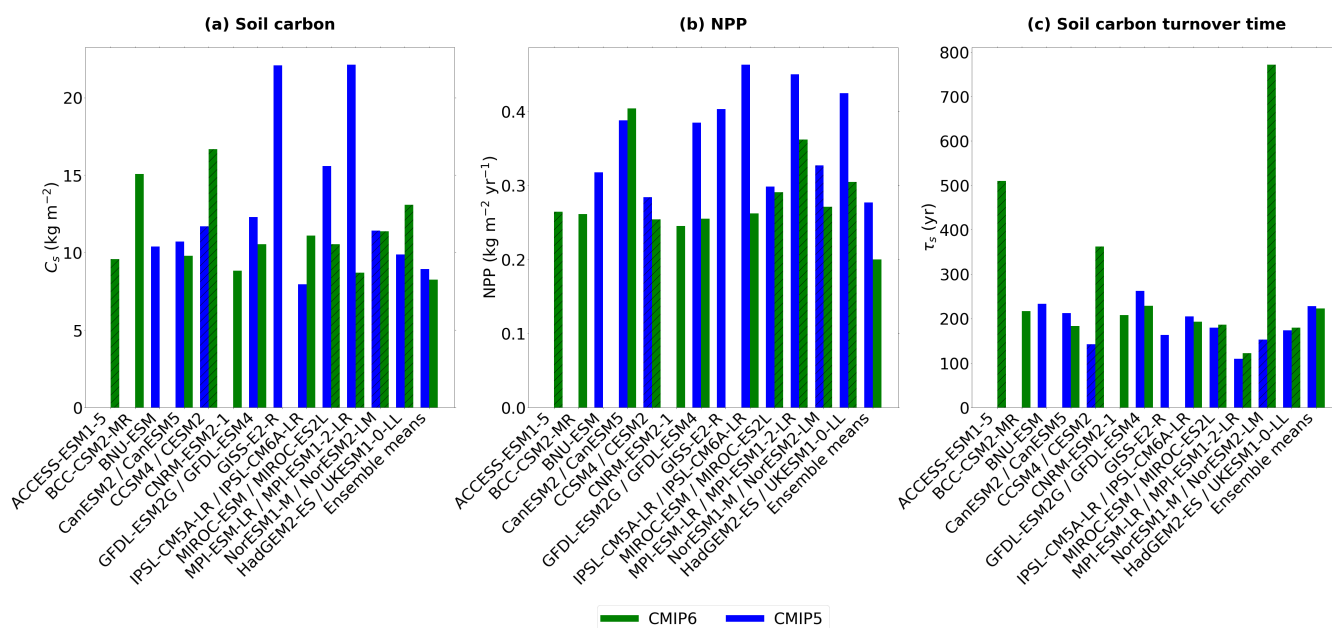


**Figure 5.** Bar charts comparing the Root Mean Squared Errors (RMSEs) in CMIP6 and CMIP5, for (a) soil carbon ( $C_s$ ), (b) NPP, and (c) soil carbon turnover time ( $\tau_s$ ).

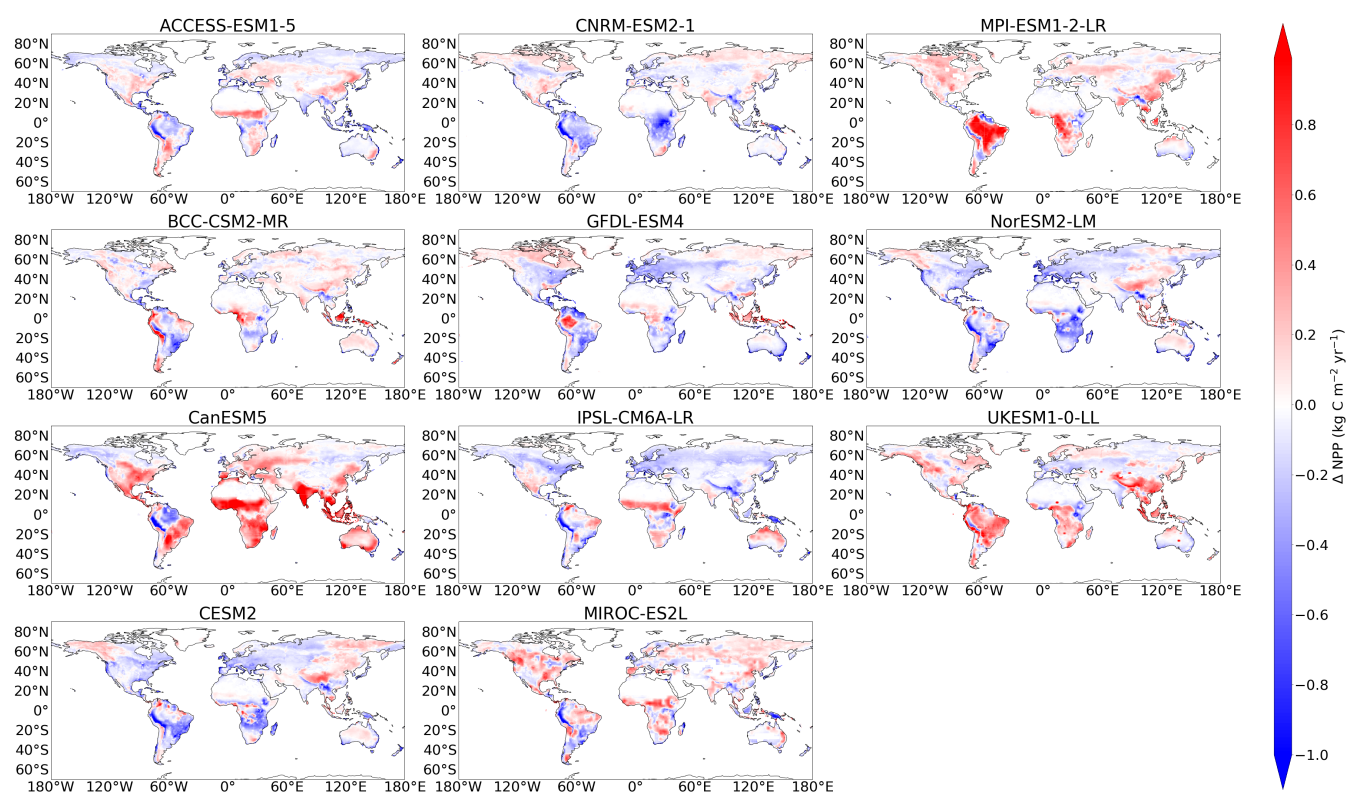


**Figure 6.** Maps of the difference in Net Primary Production (NPP) between the historical simulation of each CMIP6 model and the benchmark dataset.

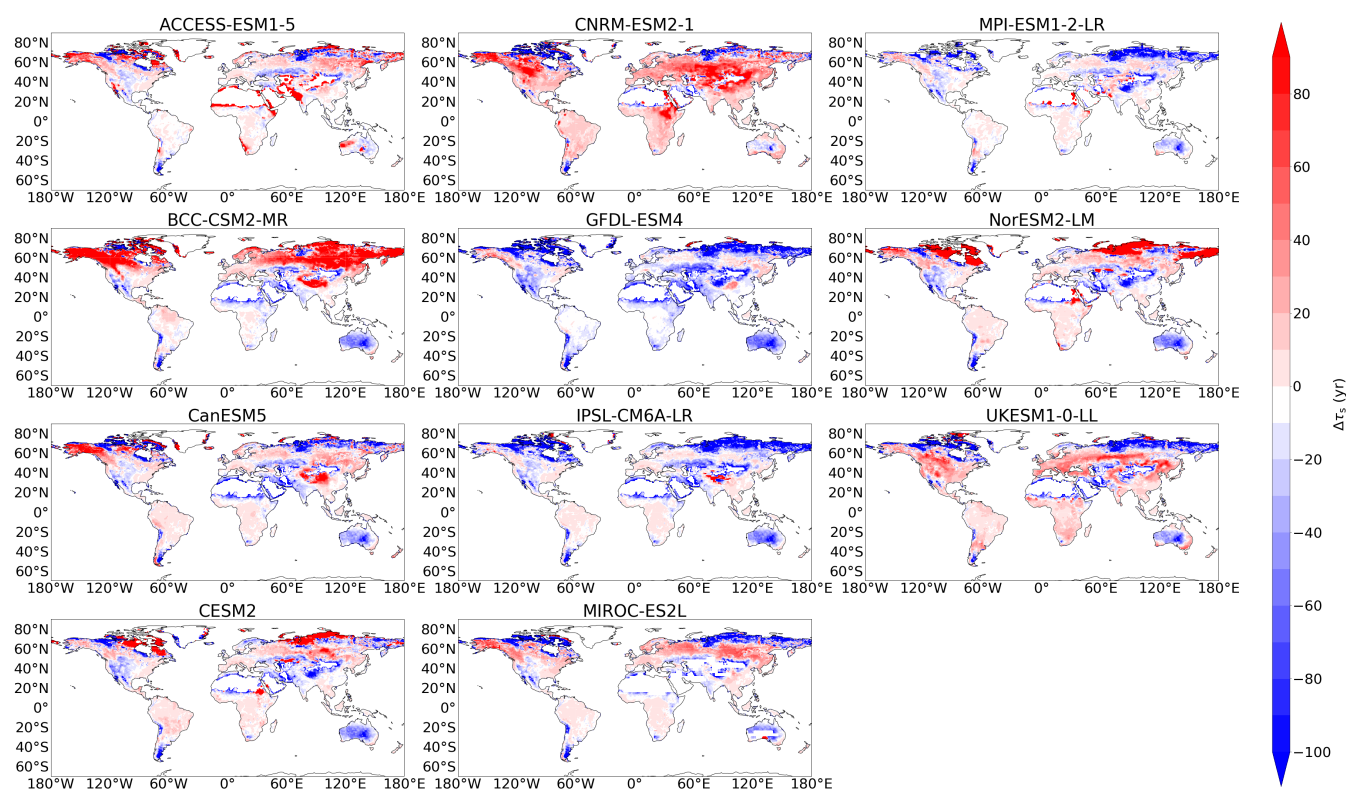


**Figure 7.** Maps of the difference in soil carbon turnover time ( $\tau_s$ ) between the historical simulation of each CMIP6 model and the benchmark datasets.

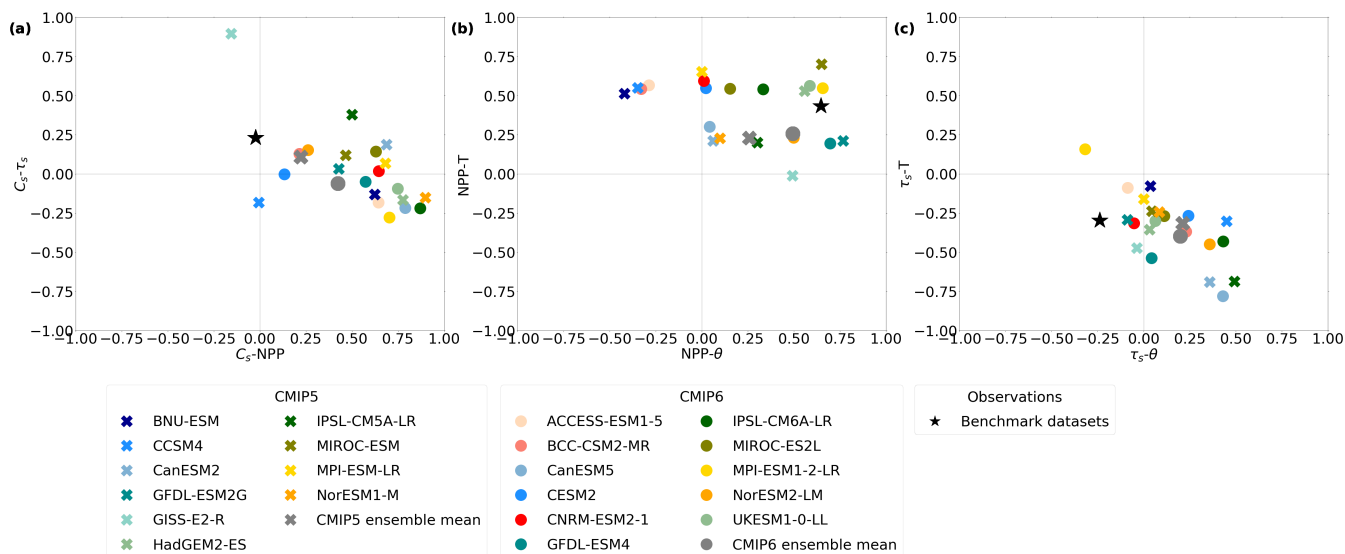


**Figure 8.** Scatter plots investigating the relationships between different Pearson correlation coefficients of climate variables, (a)  $C_s-\tau_s$  against  $C_s-NPP$ , (b)  $NPP-T$  against  $NPP-\theta$ , (c)  $\tau_s-T$  against  $\tau_s-\theta$ .

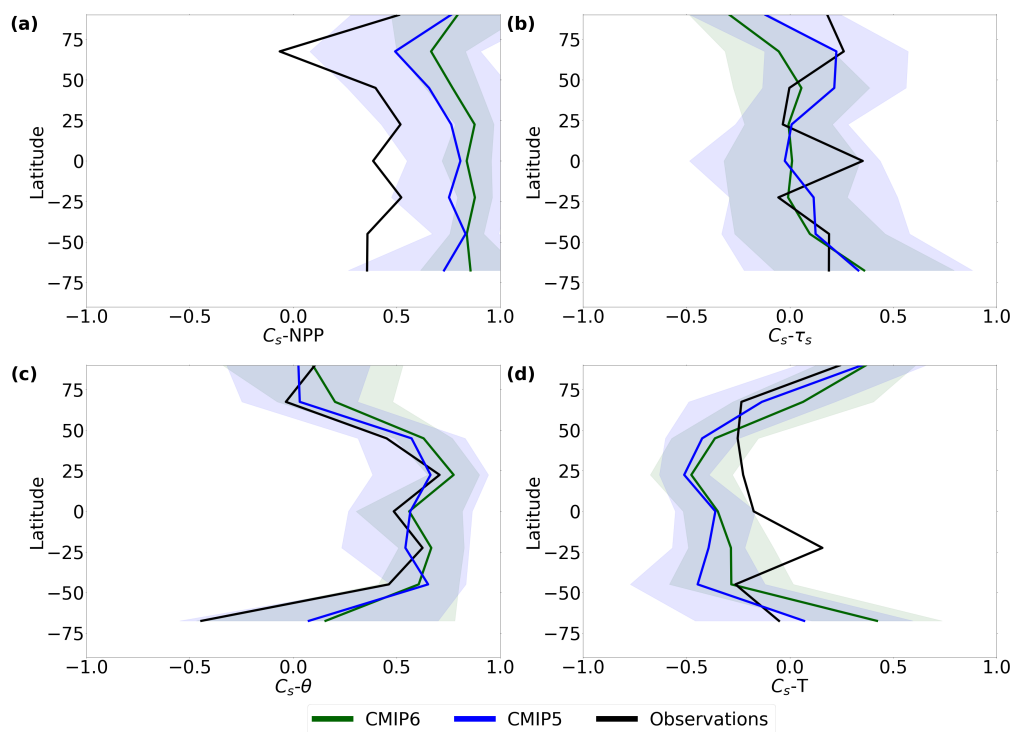


**Figure 9.** The latitudinal profiles of the Pearson correlation coefficients between soil carbon and (a) NPP ( $C_s$ -NPP), (b) soil carbon turnover time ( $C_s$ - $T_s$ ), (c) soil moisture ( $C_s$ - $\theta$ ), and (d) temperature ( $C_s$ -T).



**Table 1.** The 11 CMIP6 Earth System Models included in this study, and relevant features of their land carbon cycle components (Arora et al., 2020).

Earth System Model	Modelling Centre	Land Surface Model	Nitrogen cycle	No. of live carbon pools	No. of dead carbon pools	Temperature & Moisture	References
ACCESS-ESM1.5	CSIRO	CABLE2.4 + CASA-CNP	Yes	3	6	Arrhenius & Hill	Ziehn et al. (2020) Haverd et al. (2018) Trudinger et al. (2016)
BCC-CSM2-MR	BCC	BCC-AVIM2	No	3	8	Hill & Hill	Wu et al. (2019) Ji et al. (2008)
CanESM5	CCCma	CLASS-CTEM	No	3	2	$Q_{10}$ & Hill	Swart et al. (2019) Melton et al. (2020) Seiler et al. (2021)
CESM2	CESM	CLM5	Yes	22	7	Arrhenius & Increasing	Danabasoglu et al. (2020) Lawrence et al. (2019)
CNRM-ESM2-1	CNRM	ISBA-CTrip	No	6	7	$Q_{10}$ & Increasing	Séférián et al. (2019) Delire et al. (2020)
GFDL-ESM4	GFDL	LM4.1	No	6	4	Hill & Increasing	Dunne et al. (2020) Zhao et al. (2018)
IPSL-CM6A-LR	IPSL	ORCHIDEE branch 2.0	No	8	3	$Q_{10}$ & Increasing	Boucher et al. (2020) Cheruy et al. (2020) Guimberteau et al. (2018)
MIROC-ES2L	JAMSTEC	MATSIRO VISIT-s	Yes	3	6	Arrhenius & Increasing	Hajima et al. (2020) Ito and Oikawa (2002)
MPI-ESM1.2-LR	MPI	JSBACH3.2	Yes	3	18	$Q_{10}$ & Increasing	Mauritsen et al. (2019) Goll et al. (2017) Goll et al. (2015)
NorESM2-LM	NCC	CLM5	Yes	22	7	Arrhenius & Increasing	Seland et al. (2020) Lawrence et al. (2019)
UKESM1-0-LL	UK	JULES-ES-1.0	Yes	3	4	$Q_{10}$ & Hill	Sellar et al. (2020) Wiltshire et al. (2021)



**Table 2.** The 10 CMIP5 Earth System Models included in this study, and relevant features of their land carbon cycle components (Arora et al., 2013; Anav et al., 2013; Friedlingstein et al., 2014). Including temperature and moisture functions presented in Todd-Brown et al. (2013).

Earth System Model	Modelling Centre	Land Surface Model	Nitrogen cycle	No. of live & dead carbon pools	Temperature & Moisture	References
BNU-ESM	BNU	CoLM + BNU-DGVM	Yes	-	$Q_{10}$ & Increasing	Ji et al. (2014) Dai et al. (2003)
CCSM4	CCSM	CLM4	Yes	20	Arrhenius & Increasing	Gent et al. (2011) Lawrence et al. (2011)
CanESM2	CCCma	CLASS2.7 + CTEM1	No	5	$Q_{10}$ & Hill	Arora et al. (2009) Arora and Boer (2010)
GFDL-ESM2G	GFDL	LM3	No	10	Hill & Increasing	Dunne et al. (2012) Dunne et al. (2013) Shevliakova et al. (2009)
GISS-E2-R	NASA-GISS	YIBs, version 1.0	No	12	Increasing & Increasing	Schmidt et al. (2014) Yue and Unger (2015)
HadGEM2-ES	MOHC	JULES + TRIFFID	No	7	$Q_{10}$ & Hill	Jones et al. (2011) Best et al. (2011) Clark et al. (2011)
IPSL-CM5A-LR	IPSL	ORCHIDEE	No	7	$Q_{10}$ & Increasing	Dufresne et al. (2013) Krinner et al. (2005)
MIROC-ESM	JAMSTEC	MATSIRO + SEIB-DGVM	No	6	Arrhenius & Increasing	Watanabe et al. (2011) Ito and Oikawa (2002) Sato et al. (2007)
MPI-ESM-LR	MPI	JSBACH + BETHY	No	6	$Q_{10}$ & Increasing	Raddatz et al. (2007) Knorr (2000)
NorESM1-M	NCC	CLM4	Yes	20	Arrhenius & Increasing	Bentsen et al. (2013) Iversen et al. (2013) Lawrence et al. (2011)



**Table 3.** Table of global total and northern latitude total (northern latitudes defined as 60° N - 90° N) soil carbon estimates from multiple empirical datasets, for varying soil depths where applicable.

Empirical dataset	Depth	Global total $C_s$ (PgC)	Northern latitude total $C_s$ (PgC)	Reference
HWSD + NCSCD	1m	1412 ± 215	401 ± 61	FAO and ISRIC (2012) Hugelius et al. (2013)
WISE30sec	1m	1371 ± 129	314	Batjes (2016)
	2m	1952 ± 198	468	
S2017	1m	1966	515	Sanderman et al. (2017)
	2m	3141	893	
GSDE	1m	1682	526	Shangguan et al. (2014)
	2.3m	2593	849	
IGBP DIS	1m	1567	377	IGBP (2000)



**Table 4.** Table presenting global soil carbon values for the 11 CMIP6 models included in this study and the benchmark datasets. Including: global total  $C_s$  in PgC, and northern latitude total ( $90^\circ\text{N} - 60^\circ\text{N}$ )  $C_s$  in PgC, and the spatial mean value of  $C_s$  and corresponding standard deviation in  $\text{kg m}^{-2}$ .

Earth System Model	Global total $C_s$ (PgC)	Northern latitude total $C_s$ (PgC)	Mean $C_s \pm \text{std}$ ( $\text{kg m}^{-2}$ )
ACCESS-ESM1.5	900	151	$5.86 \pm 5.35$
BCC-CSM2-MR	1770	575	$11.6 \pm 16.6$
CanESM5	1500	218	$3.87 \pm 6.52$
CESM2 (cSoilAbove1m)	991	294	$7.05 \pm 16.6$
<i>CESM2 (cSoil)</i>	<i>1870</i>	<i>1036</i>	<i><math>13.8 \pm 51.7</math></i>
CNRM-ESM2-1	1810	440	$12.2 \pm 9.98$
GFDL-ESM4	516	163	$1.36 \pm 3.43$
IPSL-CM6A-LR	639	66.0	$4.80 \pm 3.37$
MIROC-ES2L	1460	347	$9.31 \pm 10.7$
MPI-ESM1.2-LR	970	175	$6.68 \pm 5.23$
NorESM2-LM (cSoilAbove1m)	969	300	$2.61 \pm 6.97$
<i>NorESM2-LM (cSoil)</i>	<i>2430</i>	<i>1563</i>	<i><math>6.60 \pm 41.3</math></i>
UKESM1-0-LL	1760	194	$12.0 \pm 10.9$
Ensemble mean	$1206 \pm 445$	$266 \pm 139$	$2.80 \pm 5.15$
Benchmark dataset	$1412 \pm 215$	$401 \pm 83$	$10.7 \pm 9.28$



**Table 5.** Table presenting global soil carbon values for the 10 CMIP5 models included in this study and the benchmark datasets. Including: global total  $C_s$  in PgC, and northern latitude total ( $90^\circ\text{N} - 60^\circ\text{N}$ )  $C_s$  in PgC, and the spatial mean value of  $C_s$  and corresponding standard deviation in  $\text{kg m}^{-2}$ .

Earth System Model	Global total $C_s$ (PgC)	Northern latitude total $C_s$ (PgC)	Mean $C_s \pm \text{std}$ ( $\text{kg m}^{-2}$ )
BNU-ESM	681	135	$5.31 \pm 4.55$
CCSM4	507	28.1	$4.03 \pm 3.24$
CanESM2	1540	300	$9.16 \pm 9.11$
GFDL-ESM2G	1420	635	$9.47 \pm 13.2$
GISS-E2-R	2150	609	$15.9 \pm 20.8$
HadGEM2-ES	1080	148	$8.19 \pm 6.24$
IPSL-CM5A-LR	1350	346	$9.77 \pm 7.64$
MIROC-ESM	2550	742	$20.5 \pm 15.1$
MPI-ESM-LR	3000	204	$23.5 \pm 14.8$
NorESM1-M	538	31.0	$3.61 \pm 3.34$
Ensemble mean	$1480 \pm 810$	$318 \pm 246$	$10.5 \pm 6.02$
Benchmark dataset	$1412 \pm 215$	$401 \pm 83$	$10.7 \pm 9.28$



**Table 6.** Table presenting global carbon fluxes and turnover time values for the 11 CMIP6 models included in this study and the benchmark datasets. Including: global total NPP ( $\text{PgC yr}^{-1}$ ) and effective average soil carbon turnover time (yr).

Earth System Model	NPP ( $\text{PgC yr}^{-1}$ )	$\tau_s$ (yr)
ACCESS-ESM1.5	45.6	19.0
BCC-CSM2-MR	51.2	34.1
CanESM5	75.5	18.1
CESM2 (cSoilAbove1m)	43.9	25.8
<i>CESM2 (cSoil)</i>	-	50.4
CNRM-ESM2-1	45.6	41.5
GFDL-ESM4	52.6	11.2
IPSL-CM6A-LR	46.4	14.6
MIROC-ES2L	59.1	24.5
MPI-ESM1.2-LR	58.9	15.4
NorESM2-LM (cSoilAbove1m)	43.5	24.0
<i>NorESM2-LM (cSoil)</i>	-	60.8
UKESM1-0-LL	60.8	28.1
Ensemble mean	$53.0 \pm 9.39$	$23.3 \pm 8.59$
Benchmark datasets	$56.6 \pm 14.3$	$27.0^{+27}_{-11}$



**Table 7.** Table presenting global carbon fluxes and turnover time values for the 10 CMIP5 models included in this study and the benchmark datasets. Including: global total NPP ( $\text{PgC yr}^{-1}$ ) and effective average soil carbon turnover time (yr).

Earth System Model	NPP ( $\text{PgC yr}^{-1}$ )	$\tau_s$ (yr)
BNU-ESM	44.3	16.6
CCSM4	42.9	14.3
CanESM2	59.0	72.9
GFDL-ESM2G	74.4	57.3
GISS-E2-R	31.0	47.1
HadGEM2-ES	69.1	16.8
IPSL-CM5A-LR	76.6	19.4
MIROC-ESM	47.1	56.8
MPI-ESM-LR	73.5	42.7
NorESM1-M	45.0	34.5
Ensemble mean	$56.3 \pm 15.4$	$37.8 \pm 19.7$
Benchmark datasets	$56.6 \pm 14.3$	$27.0^{+27}_{-11}$

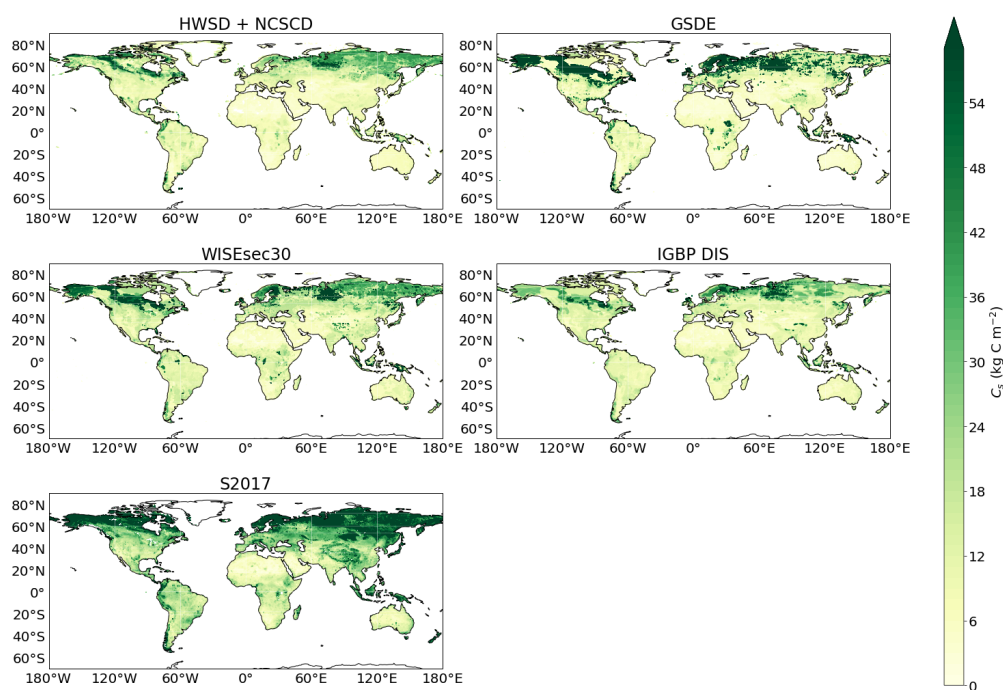


**Figure A1.** Maps comparing empirical datasets of soil carbon ( $C_s$ ). The benchmark dataset is a map plot showing  $C_s$  approximated to a depth of 1m by combining the Harmonized World Soils Database (HWSD) (FAO and ISRIC, 2012) and Northern Circumpolar Soil Carbon Database (NCSCD) (Hugelius et al., 2013), where NCSCD was used where overlap occurs. Additional map plots are shown for empirical  $C_s$  estimated by: the World Inventory of Soil property Estimates (WISE30sec) (Batjes, 2016), the named ‘S2017’ from Sanderman et al. (2017), the Global Soil Dataset for use in Earth System Models (GSDE) (Shangguan et al., 2014), and the Global Gridded Surfaces of Selected Soil Characteristics (IGBP-DIS) (IGBP, 2000).

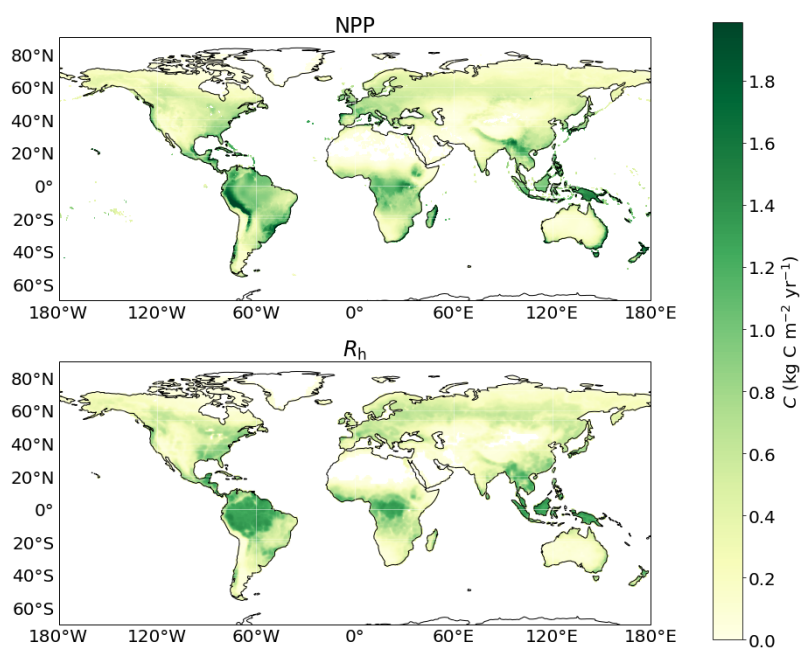


**Figure A2.** Maps of empirical carbon flux datasets. Net Primary Production (NPP) is approximated using the MODIS NPP dataset (Zhao et al., 2005), and Heterotrophic Respiration ( $R_h$ ) is approximated using the CARDAMOM  $R_h$  dataset (Bloom et al., 2015).

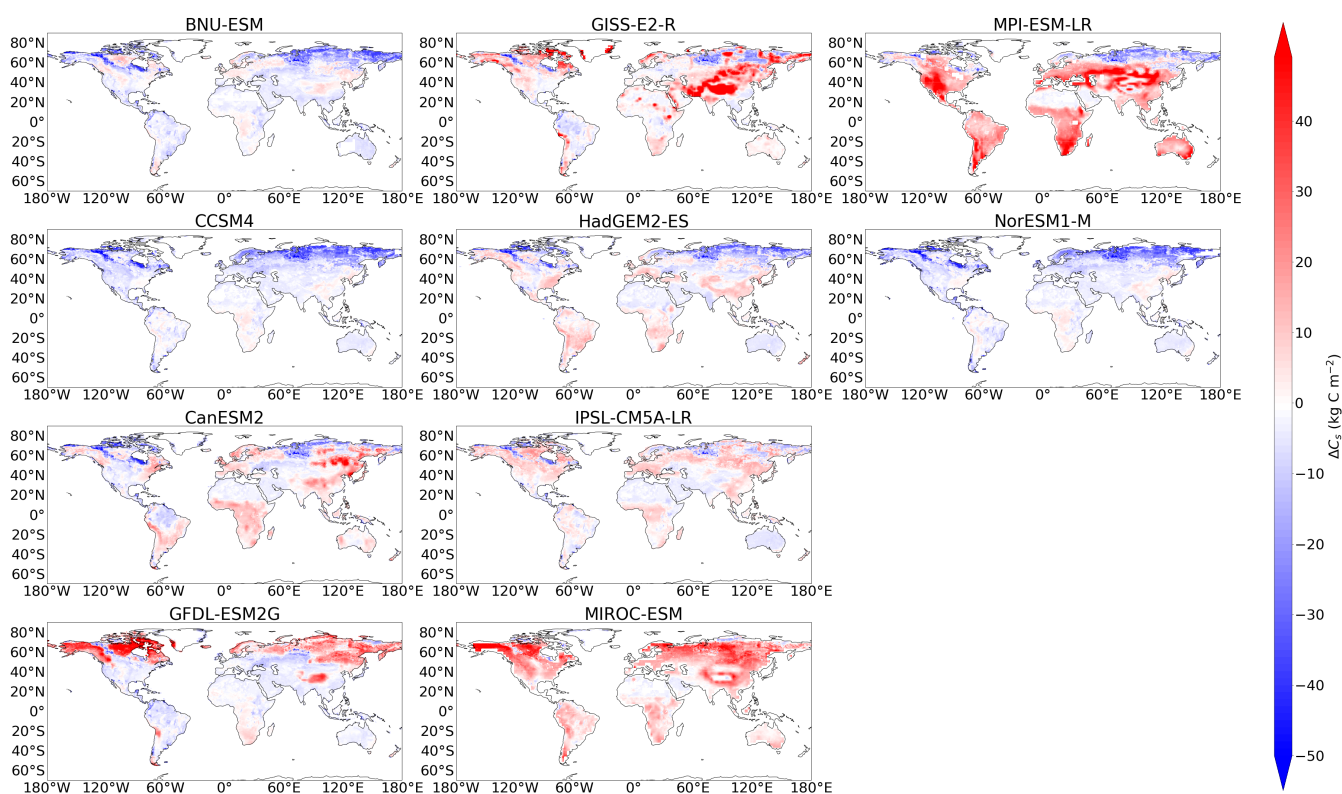


**Figure A3.** Maps of the difference in soil carbon ( $C_s$ ) between the historical simulation (1950-2000) for the CMIP5 models and the benchmark dataset.

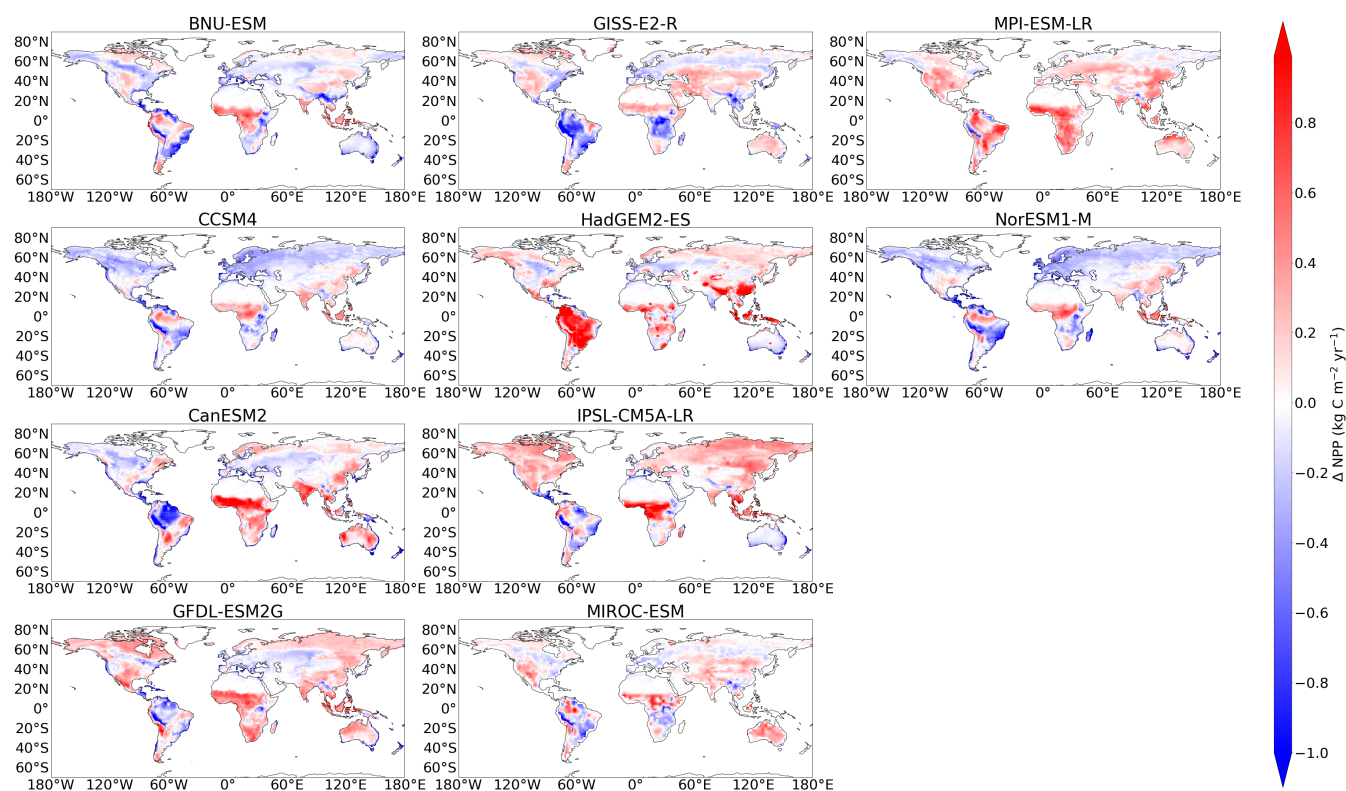


**Figure A4.** Maps of the difference in NPP between the historical simulation (1995-2005) for the CMIP5 models and the benchmark dataset.

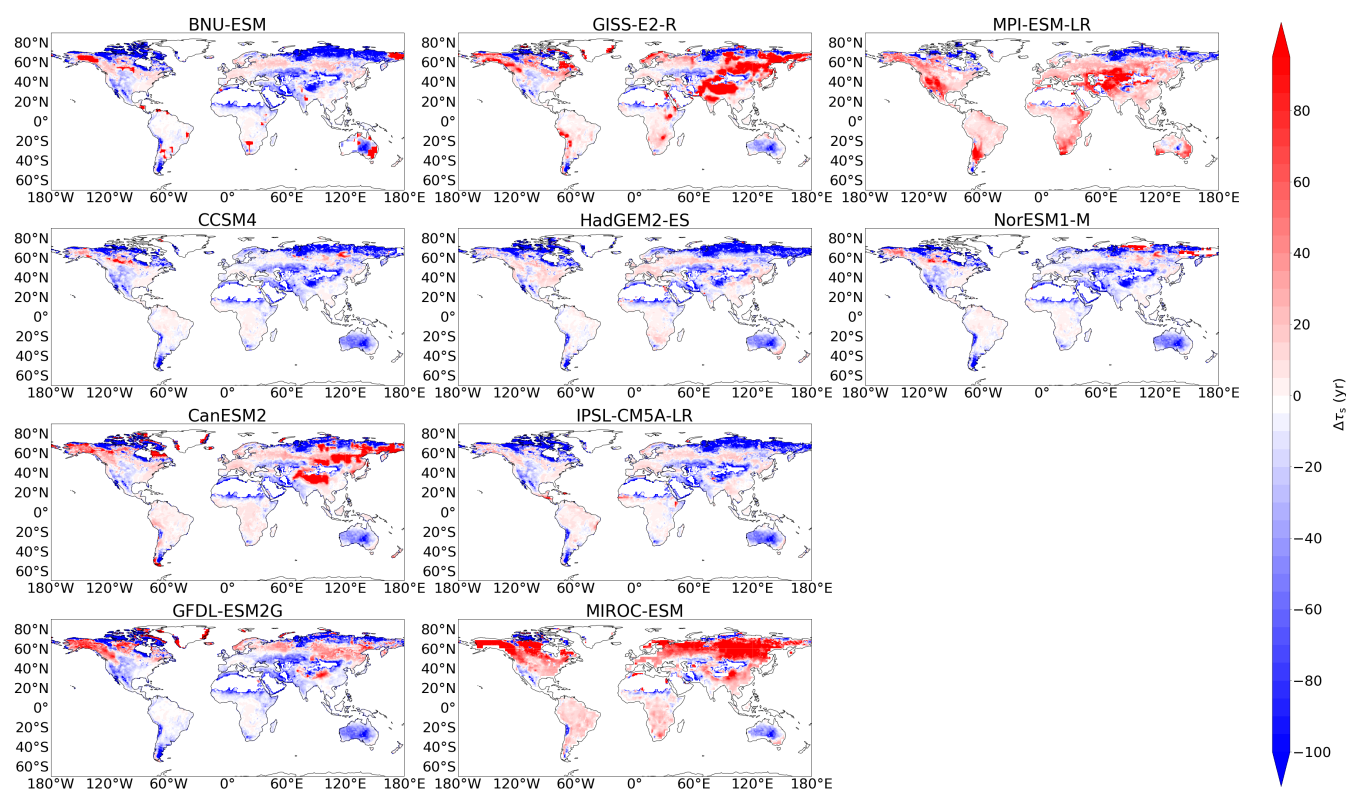


**Figure A5.** Maps of the difference in  $\tau_s$  between the historical simulation for the CMIP5 models and the benchmark datasets, where  $\tau_s$  is defined as the ratio of  $C_s$  (1950-2000) to  $R_h$  (1995-2005).



**Table A1.** Table presenting global carbon fluxes ( $\text{PgC yr}^{-1}$ ), NPP and  $R_h$ , for the 11 CMIP6 models included in this study and the empirical benchmark datasets.

Earth System Model	NPP ( $\text{PgC yr}^{-1}$ )	$R_h$ ( $\text{PgC yr}^{-1}$ )
ACCESS-ESM1.5	45.6	45.1
BCC-CSM2-MR	51.2	48.9
CanESM5	75.5	75.0
CESM2	43.9	38.3
CNRM-ESM2-1	45.6	40.3
GFDL-ESM4	52.6	43.7
IPSL-CM6A-LR	46.4	39.9
MIROC-ES2L	59.1	52.7
MPI-ESM1.2-LR	58.9	53.4
NorESM2-LM	43.5	38.2
UKESM1-0-LL	60.8	57.5
Ensemble mean	$53.0 \pm 9.39$	$48.4 \pm 10.5$
Benchmark datasets	$56.6 \pm 14.3$	$51.7 \pm 21.8$



**Table A2.** Table presenting global carbon fluxes ( $\text{PgC yr}^{-1}$ ), NPP and  $R_h$ , for the 10 CMIP5 models included in this study and the empirical benchmark datasets.

Earth System Model	NPP ( $\text{PgC yr}^{-1}$ )	$R_h$ ( $\text{PgC yr}^{-1}$ )
BNU-ESM	44.3	42.5
CCSM4	42.9	41.4
CanESM2	59.0	58.8
GFDL-ESM2G	74.4	62.7
GISS-E2-R	31.0	39.5
HadGEM2-ES	69.1	67.0
IPSL-CM5A-LR	76.6	62.4
MIROC-ESM	47.1	41.2
MPI-ESM-LR	73.5	59.9
NorESM1-M	45.0	41.3
Ensemble mean	$56.3 \pm 15.4$	$52.8 \pm 10.7$
Benchmark datasets	$56.6 \pm 14.3$	$51.7 \pm 21.8$